Dimethyl Ether as an Additive to Steam for Improved Steam-Assisted Gravity Drainage

Kai Sheng, Ryosuke Okuno, and **Mingyuan Wang,** University of Texas at Austin

Summary

Coinjection of solvent with steam results in lower chamber-edge temperatures than those in steam-assisted gravity drainage (SAGD), which enables the decrease of heat losses to the overlying formation rocks. However, use of highly volatile solvents, such as propane, can yield significantly slow bitumen production because of low chamber-edge temperatures. The suitability of alkane solvents for SAGD in terms of phase behavior has been reported to increase with increasing carbon number and tends to level off at a certain carbon number, which is approximately C_6 for Athabasca bitumen reservoirs. The main objective of this research is to investigate the potential of dimethyl ether (DME), a water-soluble solvent, as an additive to steam for reducing steam/oil ratio (SOR) while keeping SAGD-like rates of bitumen production.

The chamber-edge temperature for a given overall composition and operating pressure is defined as the temperature at which the vapor phase completely condenses with decreasing temperature. Thermodynamic predictions show that the chamber-edge temperature so defined will increase substantially if the solvent can partition into the aqueous phase at chamber-edge conditions. This is confirmed in numerical-reservoir simulation for coinjection of steam with DME, as a water-soluble solvent, for Athabasca bitumen. In simulation case studies, coinjection of steam with DME (DME-SAGD) is compared with SAGD and coinjection of steam with C_4 (C_4-SAGD), in terms of SOR, bitumen production, local displacement efficiency, and solvent recovery. The steam-injection pressure is 35 bar for all cases, and 2 mol% of solvent is coinjected in solvent-SAGD simulations until the steam chamber reaches the side boundary of a 2D homogeneous reservoir model. Because the DME volatility is between C_3 and C_4, C_4 is selected as the alkane counterpart in this simulation study to see the effect of the solvent solubility in water on oil recovery in solvent-SAGD.

DME is more volatile and less soluble in bitumen than C_4 at their corresponding chamber-edge conditions. However, results show that DME-SAGD results in 35% lower SOR than SAGD while being able to increase bitumen-production rates of SAGD. Analysis of simulation results indicates that the solubility of DME in water not only makes the chamber-edge temperature higher than that of C_4-SAGD, but also yields 15% higher solvent-recovery factor than C_4-SAGD. The main reason for the latter observation is that a much-smaller fraction of the injected solvent is present in the vapor phase in DME-SAGD than in C_4-SAGD. Also, DME dissolves in both water and bitumen, which results in the aqueous and oleic phases of nearly equal density within the gravity-drainage zone near the edge of a steam chamber. This is the neutral regime of oil/water two-phase flow along the chamber edge between the two extreme cases: SAGD and C_4-SAGD. Unlike in C_4-SAGD, the reduced gravity segregation in DME-SAGD is expected to facilitate the mixing of condensed solvent with bitumen near the edge of a steam chamber.

Introduction

In-situ recovery of heavy oil and bitumen is challenging because they are highly viscous, and usually are immobile at reservoir conditions (Butler 1997). SAGD is the most widely used method of bitumen recovery. In SAGD, steam is injected into the bitumen reservoir through an (upper) horizontal well and forms a steam-saturated zone, which is called a "steam chamber." At the edge of a steam chamber, the vapor (V) phase completely condenses, and releases its latent heat. The heated oil and steam condensate drain by gravity to the (lower) horizontal well that is 4 to 8 m below and parallel to the injection well. Although only a part of the heat can be added to the oleic (L) phase in the reservoir, it effectively increases the L-phase mobility because viscosity of bitumen is highly sensitive to temperature. The main drawback of SAGD is the significant use of energy and water to generate steam, which also results in a large amount of greenhouse-gas emission.

A widely used parameter to quantify the energy efficiency of steam-injection processes is the cumulative steam/oil ratio (CSOR), defined as the ratio of the cumulative volume of steam injected (cold water equivalent) to the cumulative volume of bitumen produced. CSOR is particularly sensitive to heat losses to the overlying formation rocks. In SAGD, elevated temperatures (e.g., 450 to 520 K) occur within the steam chamber and in regions beyond the chamber edge in its vicinity. Shen (2013) stated that, for SAGD to be economically feasible, the energy efficiency measured by CSOR is generally in the range of 2 to 4 m^3/m^3. It is desirable to operate at low chamber temperatures while maintaining economically sustainable rates of oil production so that the CSOR can be reduced. SAGD is expected to be even less energy-efficient for highly heterogeneous reservoirs (Venkatramani and Okuno 2017). Thus, there is a critical need to reduce the SAGD CSOR from both environmental and economic standpoints, which has motivated the search for alternative processes.

Coinjection of steam and solvent for SAGD (solvent-SAGD) has been studied and pilot tested as a potential method to improve the drawbacks of SAGD (Leaute 2002; Gupta et al. 2005; Leaute and Carey 2007; Gupta and Gittins 2006). Solvent-SAGD processes proposed in the literature, such as expanding-solvent SAGD (ES-SAGD), solvent-aided process, and liquid addition to steam for enhanced recovery (LASER), use a small amount of solvents (e.g., a few to 20% by liquid volume equivalent) (Leaute 2002; Gupta et al. 2005; Leaute and Carey 2007; Gupta and Gittins 2006). They attempt to enhance the L-phase mobility by the dilution of oil by solvent, in addition to the thermal energy released from the injected steam, to reduce the steam requirement. It is reported in the literature that solvent-SAGD, if properly designed, can increase bitumen-drainage rate and displacement efficiency while reducing CSOR (e.g., the EnCana solvent-aided-process pilot and the Imperial Oil LASER) (Nasr et al. 2003; Gates 2007; Gupta et al. 2005; Gupta and Gittins 2006; Leaute 2002; Leaute and Carey 2007; Li et al. 2011a b; Keshavarz et al. 2014, 2015).

This paper (SPE 184983) was accepted for presentation at the SPE Canada Heavy Oil Technical Conference, Calgary, 15–16 February 2017, and revised for publication. Original manuscript received for review 31 December 2016. Revised manuscript received for review 14 October 2017. Paper peer approved 17 October 2017.

Prior investigations into solvent-SAGD are mainly concerned with hydrocarbon solvents, such as propane, butane, and diluents, which usually consist of pentane and heavier hydrocarbons at different concentrations (Nasr et al. 2003; Gates 2007; Ivory et al. 2008; Li et al. 2011a, b; Keshavarz et al. 2014, 2015). The hydrocarbon solvents that are reported to be suitable have vapor pressures that are close to that of water at an operating pressure; e.g., *n*-hexane and *n*-heptane as single-component solvents for various bitumen reservoirs (Li et al. 2011a; Mohebati et al. 2012; Keshavarz et al. 2015). However, such hydrocarbon solvents are relatively expensive, and in-situ retention of the coinjected solvent, which inevitably happens under heterogeneity, can substantially affect the project economics.

In general, more-volatile solvents are less expensive. Therefore, they are of lower risk for injection into bitumen/heavy-oil reservoirs. Also, it is expected that mixing of bitumen with more-volatile solvent results in lower viscosity of the resulting oil mixture at a given mixing ratio, temperature, and pressure. As will be explained in the next section, however, coinjection of steam with highly volatile solvents (e.g., propane and butane) substantially lowers the temperature at the edge of a steam chamber (in comparison with steam-only injection), which lowers the *L*-phase mobility. For example, prior investigations have shown that coinjection of propane with steam is unlikely advantageous over SAGD at the operating conditions in most target reservoirs, especially for Athabasca bitumen reservoirs (Li et al. 2011b; Keshavarz et al. 2015). Results presented in the literature show that lowering the temperature at the edge of a steam chamber by coinjection of volatile solvents with steam reduces heat losses to the overlying formation rocks, but the operating chamber-edge temperature should not be too low to maintain an SAGD-like oil-production rate (Keshavarz et al. 2014, 2015; Venkatramani and Okuno 2016). A practical way to improve the efficiency of SAGD is to develop effective strategies for solvent-SAGD that result in less consumption of energy and water while keeping an SAGD-like rate of bitumen production.

This paper is motivated by the question of how we can use the water component and/or the aqueous (*W*) phase to improve the efficiency of steam-based oil recovery, such as SAGD and cyclic steam stimulation. This is because water is by far the most dominant component in steam-based oil recovery for heavy-oil and bitumen recovery (Zhu and Okuno 2016). The volume of produced water is a few times greater than the volume of produced oil in SAGD and cyclic steam stimulation. The central hypothesis in this research is that the combined mechanisms for enhancement of bitumen mobility by heat and dilution are more effective with water-soluble solvents than with the conventional alkane-based solvents.

As will be presented in this paper for the first time, thermodynamic calculations and flow simulations using experimental data indicate that the solubility of solvent in water is expected to effectively use the thermal and compositional mechanisms for enhancing bitumen mobility in the reservoir. In this research, DME is considered as a water-soluble solvent, although it is not the purpose of this paper to single out DME as a promising additive to steam to improve SAGD.

DME is the lightest organic in the ether family with the chemical formula of CH_3-O-CH_3. DME can be synthesized in a variety of ways at low costs, such as from methanol, organic waste, and biomass. The second lightest ether is diethyl ether, but it is highly reactive. Therefore, DME is the only ether considered in this research.

DME is a colorless gas with mild sweet odor at standard conditions. It liquefies under moderate pressure or cooling (Ratnakar et al. 2016a). DME is between propane (C_3) and *n*-butane (C_4) in terms of volatility, and soluble in oil as presented in the experimental studies (Ihmels and Lemmon 2007; Wu and Yin 2008). Other properties of DME, such as density, viscosity, and critical parameters, are reported in the literature (Wu et al. 2003, 2004; Ihmels et al. 2007). Because of its slight polarity, DME is also soluble in water (Ratnakar et al. 2016a, b). However, there are a limited amount of experimental data for DME/water and DME/oil mixtures. Experimental studies of DME/water binary-phase behavior were presented by Pozo and Streett (1984) and Holldorff and Knapp (1988). Park et al. (2007) conducted an experimental study for phase behavior of DME/decane and DME/dodecane mixtures. Chernetsky et al. (2015) measured densities and viscosities of DME/oil mixtures. Ratnakar et al. (2016a, b) presented phase-behavior data of DME/oil/brine. However, phase behavior of DME/bitumen/brine mixtures has not been presented in the literature.

Recently, novel applications of DME in petroleum reservoir engineering were presented in the literature. Coreflooding studies and field studies indicated that DME can be an effective solvent for enhanced-waterflooding processes (Chernetsky et al. 2015; Parsons et al. 2016; Chahardowli et al. 2016; Groot et al. 2016a, b; Alkindi et al. 2016; Te Riele et al. 2016). The DME injected can be efficiently recovered through the produced water because of the solubility in water, and the produced water that contains DME can be reused (Chernetsky et al. 2015; Parsons et al. 2016). Furthermore, Ganjdanesh et al. (2016) showed that DME can be used to treat condensate and water blocks in hydraulic-fractured shale-gas/condensate reservoirs through numerical investigation by taking advantage of DME distribution in the *W* and *L* phases and its high volatility.

Thermodynamic modeling for the application of DME to petroleum-engineering processes has been studied. Cubic equations of state (EOSs), such as the Peng-Robinson (PR) EOS (Robinson and Peng 1978), with the van der Waals (vdW) mixing rules are not entirely satisfactory for modeling DME/water mixtures (Ratnakar et al. 2016a, b). Accurate modeling of hydrogen bonding and polar interactions usually requires more-advanced EOSs and/or mixing rules, such as cubic-plus-association EOS and the Huron and Vidal (HV) (1979) mixing rule (Chapman et al. 1986; Michelsen 1990; Kontogeorgis et al. 1996; Folas et al. 2006a, b; Oliveira et al. 2007; Pedersen et al. 2014; Ratnakar et al. 2016a, b). Ratnakar et al. (2016a) used the CPA EOS based on Soave-Redlich-Kwong (Soave 1972) to calculate partitioning of DME in the *W* and *L* phases for DME/oil/brine mixtures. Ratnakar et al. (2016b) used the PR EOS with the HV mixing rule to model phase behavior of DME/brine/oil mixtures.

The primary objective of this paper is to present, for the first time, potential benefits of using DME, a water-soluble solvent, as a steam additive to improve the efficiency of SAGD, along with the mechanisms involved. To study the effect of the solvent solubility in water on oil recovery in solvent-SAGD, the secondary objective is to compare DME/steam coinjection (DME-SAGD) with coinjection of steam with volatile alkanes, such as C_4, of which the volatility is close to DME. The research is based on thermodynamic calculations and flow simulations; however, experimental data available for relevant fluids are used to calibrate the numerical models. The significance of the paper lies in the mechanistic explanation of how the DME solubility in water is expected to make differences in temperature and component distributions during SAGD and its variants. Optimal conditions for DME-SAGD are beyond the scope of the current paper because DME has been taken merely as an example of a water-soluble solvent.

The next section presents thermodynamic calculations for chamber-edge conditions for SAGD and solvent-SAGD with different solvents, such as DME and alkanes. This will explain the effect of the solvent solubility in water on chamber-edge conditions. Then, a simulation case study will compare SAGD and solvent-SAGD with DME and C_4 in terms of bitumen-production rate, CSOR, ultimate bitumen recovery, and solvent recovery.

Vapor-Condensation Conditions for Water/Solvent/Bitumen

Oil drainage by gravity occurs mainly along the edge of a steam chamber in SAGD and its variants (Keshavarz et al. 2014). Therefore, the temperature-composition conditions near the steam-chamber edge substantially affect the efficiency of solvent-SAGD in terms of oil production and energy/water consumption at a given operating pressure (Keshavarz et al. 2014, 2015; Venkatramani and Okuno

2016). In general, there are three phases inside a steam chamber: the vapor (*V*), aqueous (*W*), and oleic (*L*) phases. At the edge of a steam chamber, the *V* phase completely condenses, making hot water (water condensate) from the vapor water and liquid solvent from the vapor solvent. This liquid solvent is then mixed with heated, mobile bitumen through mechanical dispersion along and outside the edge of a steam chamber (Venkatramani and Okuno 2017). In solvent-SAGD, therefore, the *L*-phase mobility becomes higher not only by the thermal mechanism, but also by the compositional mechanism.

The thermodynamic conditions at the edge of a steam chamber in solvent-SAGD depend substantially on the phase behavior of water/solvent/bitumen mixtures (Keshavarz et al. 2014, 2015; Venkatramani and Okuno 2016). More specifically, such conditions are determined by vapor condensation, in which a phase transition occurs between two phases (*WL*) and three phases (*WLV*), in the water/solvent/bitumen system at a given operating pressure and overall composition. **Fig. 1** schematically illustrates the chamber-edge (or vapor-condensation) conditions in a ternary diagram for water/pentane/bitumen at a chamber-edge temperature at the operating pressure of 35 bar. The red dot in the ternary diagram (Fig. 1a) indicates an overall composition on the boundary between *WL* and *WLV*, which corresponds to a point on the edge of a steam chamber (Fig. 1b) at the specified pressure.

This section provides an analysis of chamber-edge (i.e., vapor-condensation) conditions for SAGD and solvent-SAGD at a given pressure, 35 bar as an example. The solvents used for solvent-SAGD are DME and alkanes, ranging from C_3 to *n*-hexane (C_6). Ternary mixtures consisting of water, bitumen, and solvent are used in this section. First, the phase-behavior models used are described in the following two subsections. Then, the effect of water-soluble solvent (taking DME as an example) on vapor-condensation conditions are analyzed in the third subsection.

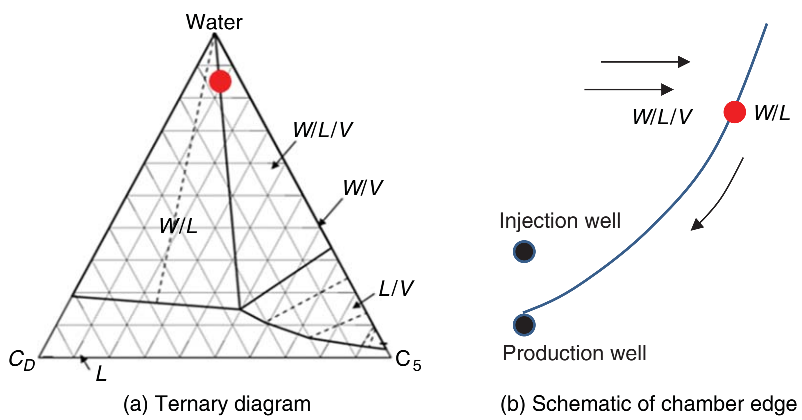

Fig. 1—Thermodynamic conditions at the edge of a steam chamber corresponding to vapor-condensation conditions. The ternary diagram shows an overall composition on the edge of a tie triangle of *W, L*, and *V* at 35 bar for the water/pentane/bitumen system as an example. C_D is the dead-oil pseudocomponent, which is bitumen in this example. The chamber schematic shows a point on the edge of a steam chamber at which the thermodynamic conditions correspond to the red dot in the ternary diagram.

EOS Model for Water/*n*-Alkane/Bitumen. The PR EOS with the vdW mixing rules is used for phase-equilibrium calculation of water/*n*-alkane/bitumen mixtures. **Tables 1 and 2** summarize parameters for the PR-EOS models with the vdW mixing rules, such as critical properties and binary-interaction parameters (BIPs). Critical properties of water and *n*-alkanes are derived from the American Petroleum Institute technical data book (API 1983) and group contribution methods (Constantinou and Gani 1994; Constantinou et al. 1995) as summarized in Venkatramani and Okuno (2015). The dead-bitumen component (C_D in Tables 1 and 2) is the Athabasca bitumen characterized by Kumar and Okuno (2016), which was described as Bitumen A in their paper.

Components	T_C (K)	P_C (bar)	ω	MW (g/mol)	$\underline{V}_C$ (cm^3/mol)
C_1	190.56	45.99	0.0157	16.04	–
C_3	369.83	42.48	0.1543	44.10	203
n-C_4	425.12	37.96	0.2014	58.12	255
n-C_5	469.70	33.70	0.2511	72.15	304
n-C_6	507.60	30.25	0.3010	86.18	370
C_D	847.17	10.64	1.0406	530.00	1330
Water	647.10	220.64	0.3433	18.01	–
DME	400.05	52.92	0.2000	46.07	–

Table 1—Critical properties and molecular weight (MW) for components.

A BIP correlation for water with alkanes was developed for reliable estimation of water solubility in alkanes using the PR EOS (Robinson and Peng 1978; Venkatramani and Okuno 2015):

$$BIP_{w/HC} = c_1[1 + \exp(c_2 - c_3 MW)]^{-1/c_4}, \quad (1)$$

where $c_1 = 0.24200$, $c_2 = 65.90912$, $c_3 = 0.18959$, and $c_4 = -56.81257$. *MW* is the molecular weight (in g/mol) of *n*-alkane. This correlation is dependent on experimental data for water/alkane three-phase behavior (Brunner 1990). This BIP correlation with the PR EOS gave accurate estimation of three-phase temperatures for water with *n*-alkanes from C_3 to C_{36} and water solubilities in alkanes from C_3

to C_{20} with average absolute deviations (AADs) of 1.7 K and 4.2 mol%, respectively (Venkatramani and Okuno 2015). For the BIP of water with C_D, the value from Eq. 1 is multiplied by 0.7 to account for the effect of aromaticity of the bitumen (C_D) on the solubility of water in bitumen. The scaling factor of 0.7 was obtained by Venkatramani and Okuno (2016) by matching experimental data for Athabasca bitumen measured by Amani et al. (2013a, b).

BIP	C_1	C_3	n-C_4	n-C_5	n-C_6	C_D
C_D	0.000	0.067	0.075	0.081	0.088	0.000
Water	0.732	0.666	0.636	0.607	0.579	0.169
DME	0.000	0.000	0.000	0.000	0.000	0.015

Table 2—BIPs for the PR EOS with the vdW mixing rules. All other BIPs are zero. C_D stands for the dead-bitumen component. The vdW mixing rules are used for all the binaries in water/n-alkane/bitumen mixtures, and for the water/bitumen and bitumen/DME binary pairs in water/DME/bitumen mixtures.

The solubility of alkanes in water has been measured to be very low; e.g., up to 0.1 mol% as reported by Scharlin et al. (1998). For example, Reamer et al. (1952) showed the solubility of C_4 in water at 511 K and 68.9 bar was 0.0792 mol%. The PR EOS with the BIP correlation given in Eq. 1 usually underestimates the solubility of alkanes in water (Venkatramani and Okuno 2015); that is, alkanes are essentially insoluble in water, and partition only into the vapor and oleic phases in this research.

The small solubility of C_4 in water has marginal effects on phase behavior in this research. For example, the PR-EOS models for water/C_4 using the HV mixing rule (Ratnakar et al. 2016b) and the vdW mixing rules (Venkatramani and Okuno 2015) respectively yield 0.084 mol% and 0.000 mol% for the C_4 solubility in water at 511 K and 68.9 bar. The resulting W-phase densities in the STARS (CMG 2014) simulator are 807.0 kg/m^3 and 806.9 kg/m^3 with the HV and vdW models, respectively.

BIPs between bitumen and n-alkanes are calculated by the following correlation (Kumar 2016):

$$BIP_{\text{bit/sol}} = 0.0349 \ln\left(\frac{\underline{V}_{C\text{-sol}}}{\underline{V}_{C\text{-bit}}}\right) + 0.1329, \quad (2)$$

where $\underline{V}_C$ is critical molar volume, $\underline{V}_{C\text{-sol}}$ is the standard value for the alkane solvent of interest, and $\underline{V}_{C\text{-bit}}$ can be calculated directly from the Riazi and Daubert (1987) correlation.

EOS Model for Water/DME/Bitumen. The vdW mixing rules are inaccurate for modeling water/DME mixtures, especially for three-phase conditions and solubility of DME in water. For example, if the PR EOS with the vdW mixing rules is calibrated with three-phase conditions for water/DME mixtures (Pozo and Streett 1984), the average absolute relative deviation (AARD) for the DME solubility in water is more than 45% dependent on Pozo and Streett (1984). The HV mixing rule (Huron and Vidal 1979) is more flexible than the vdW mixing rules for modeling mixtures with polarity and hydrogen bonding (Kontogeorgis and Folas 2009). Therefore, the PR EOS with the HV mixing rule is used for modeling water/DME/bitumen mixtures in this research; the vdW mixing rules are used for the water/bitumen and bitumen/DME binary pairs; and the HV mixing rule is used for the water/DME binary pair. Ratnakar et al. (2016b) used the HV mixing rule for calibrating a DME/brine/oil system with experimental data and predicting the partitioning of DME into the L and W phases.

Properties of water and C_D are the same as in the water/n-alkane/bitumen models. Vapor-pressure data for DME, such as critical temperature (T_C), critical pressure (P_C), and acentric factor (ω), were taken from Tallon and Fenton (2010), as shown in Table 1. However, experimental data for mixtures of DME with other components are scarce. As explained here, therefore, interaction parameters for DME/C_D (Table 2) and water/DME were calibrated with experimental data.

For DME/hydrocarbon mixtures, the only data that are relevant to this research and available in the literature are given by Park et al. (2007) for the DME solubility in n-decane (C_{10}) and n-dodecane (C_{12}). A BIP of 0.015 has been found to give an AARD of 1.5% for these data. Although the BIP of DME with bitumen is expected to be different, 0.015 is also used for the DME/C_D pair in the absence of any other relevant data (Table 2).

The HV parameters for the water/DME pair were obtained by matching the data for three-phase conditions and DME solubility in water up to 493 K and 509 bar (Pozo and Streett 1984). The randomness parameters for components j and k are 0.131 for the two ways (jk and kj), where j is water and k is DME. The energy parameters for j (water) and k (DME) are $g_{jk}/R = g'_{jk}/R + Tg''_{jk}/R$, where g'_{jk}/R is –1000 K and g''_{jk}/R is –0.570, and $g_{kj}/R = g'_{kj}/R + Tg''_{kj}/R$, where g'_{kj}/R is 1370 K and g''_{kj}/R is 1.290. R is the universal gas constant.

Unlike the vdW mixing rules, the HV mixing rule exhibits improved accuracy for DME solubility in water and three-phase conditions. AARDs for three-phase temperature and DME solubility in water with the HV mixing rule are 0.9% and 17.3%, respectively. The corresponding AAD is 3.8 K for three-phase temperature and 2.1 mol% for DME solubility in water on the three-phase curve. **Fig. 2** also compares EOS predictions with experimental data of Pozo and Streett (1984). In Fig. 2, the horizontal line for each temperature represents the three-phase pressure for the W, V, and L phases. Above the three-phase pressure, two different two-phase regions (W/L and L/W) are present (not shown in Fig. 2). Below it, the W/V region is present.

Analysis of Vapor-Condensation Temperature at 35 bar. This subsection presents the difference between alkanes and DME in terms of phase behavior when they are mixed with water and bitumen at a given pressure, 35 bar, using the EOS models (see the two preceding subsections). Differences come from the solubility in water, which is much greater for DME than for alkanes (Fig. 2). The main objective in this subsection is to explain the potential effect of this difference on vapor-condensation (or chamber-edge) temperature for water/solvent/bitumen mixtures in solvent-SAGD.

Fig. 3 shows vapor-pressure curves of solvent components and three-phase curves for water/solvent binaries using the EOS models described in the two preceding subsections. Vapor-pressure curves in Fig. 3 show that DME is between C_3 and C_4 in terms of volatility. However, the interaction of DME with water is apparently different from that of n-alkanes with water. For example, the three-phase curve for the water/DME binary is on the higher-temperature side of the DME vapor-pressure curve (Pozo and Streett 1984). However, the three-phase curve for a water/n-alkane binary is observed to be on the lower-temperature side of the vapor-pressure curve for that of n-alkane (Brunner 1990).

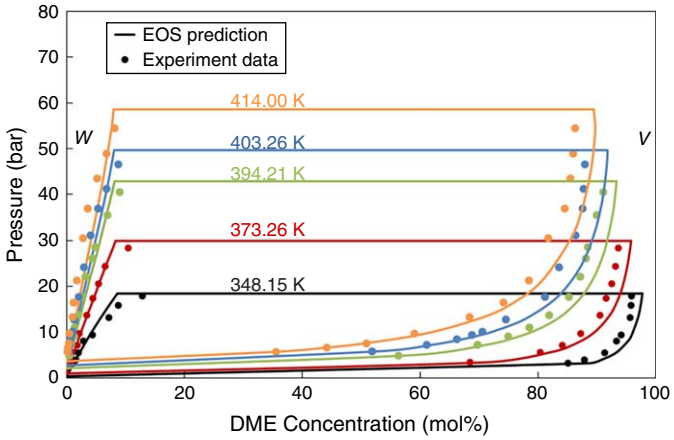

Fig. 2—Pressure/composition (*Px*) diagrams for water/DME mixtures at five different temperatures. The data were taken from Pozo and Streett (1984). The predictions are based on the PR EOS with the HV mixing rule. The horizontal line for each temperature represents the three-phase conditions for the *W, V,* and *L* phases.

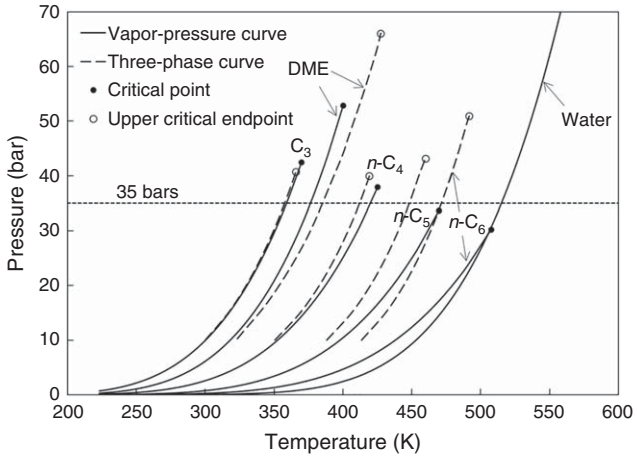

Fig. 3—Vapor-pressure curves of pure components and three-phase curves for water/solvent binaries. The upper critical endpoint is where three-phase behavior culminates.

Fig. 4 compares different alkane solvents in terms of vapor-condensation temperature for a typical overall composition (95 mol% water, 4 mol% solvent, and 1 mol% bitumen) for a solvent-SAGD chamber edge at 35 bar. In Fig. 4, two-phase regions associated with the tie triangle are omitted for clarity. The vapor-condensation temperature is calculated to be 358 K for propane, 415 K for butane, 453 K for pentane, and 476 K for hexane. That is, it monotonically increases with decreasing volatility of the alkane solvent used. The vapor-condensation temperature for the propane case is remarkably lower than that for the hexane case ($\Delta T = 118$ K), which substantially reduces the mobility of the resulting L phase. This largely explains the result of previous studies that *n*-hexane is more suitable than propane as an additive to steam for solvent-SAGD for Athabasca bitumen (Li et al. 2011a; Mohebati et al. 2012; Keshavarz et al. 2015).

As mentioned previously, the volatility of DME is between that of propane and butane. Therefore, one may expect that the vapor-condensation temperature can be as low as the propane and butane cases, as shown in Fig. 4. **Fig. 5** shows the ternary diagram calculated for the water/DME/bitumen system at the same conditions used for Fig. 4. The vapor-condensation temperature for the DME case is calculated to be 442 K (Fig. 5), which is higher than the propane and butane cases and even close to the pentane case (Fig. 4). Because the overall composition near the edge of a steam chamber is always in the vicinity of 100% water in SAGD and its variants, the phase-transition temperature from *WLV* to *WL* is sensitive to the solubility of solvent in water (or the composition of the *W* phase that is equilibrium with *L* and *V*) at a given operating pressure. The hypothesis obtained from these calculations is that vapor-condensation temperature at a given pressure and composition will increase substantially if the solvent can partition into the *W* phase at operating conditions. This will be confirmed in the next section through numerical reservoir simulations for coinjection of steam with different solvents, such as DME and C_4, for Athabasca bitumen at 35 bar.

Fig. 6 compares the temperature/composition (T/x) diagrams for water/C_5/C_D and water/DME/C_D at 35 bar. There are two separate three-phase regions for each diagram: $W/L_1/V$ at higher temperature and $W/L_1/L_2$ at lower temperature, where L_1 is the bitumen-rich liquid phase and L_2 is the solvent-rich liquid phase. Two-phase regions associated with the three-phase regions are not shown for clarity. The ternary diagrams given in Figs. 4 and 5 correspond to temperature cross sections inside the $W/L_1/V$ region in Fig. 6. Fig. 6 clearly shows that the lower-temperature limit for $W/L_1/V$ is substantially lower in the water/DME/C_D system than in the water/C_5/C_D system. This is a direct consequence of the difference between the three-phase temperature for water/DME and that for water/C_5 at 35 bar, which are 382.18 K and 448.37 K, respectively, as shown in Fig. 3. However, only 1 mol% of bitumen (C_D) in the overall composition makes the vapor-condensation temperature 60 K higher, as discussed with Fig. 5.

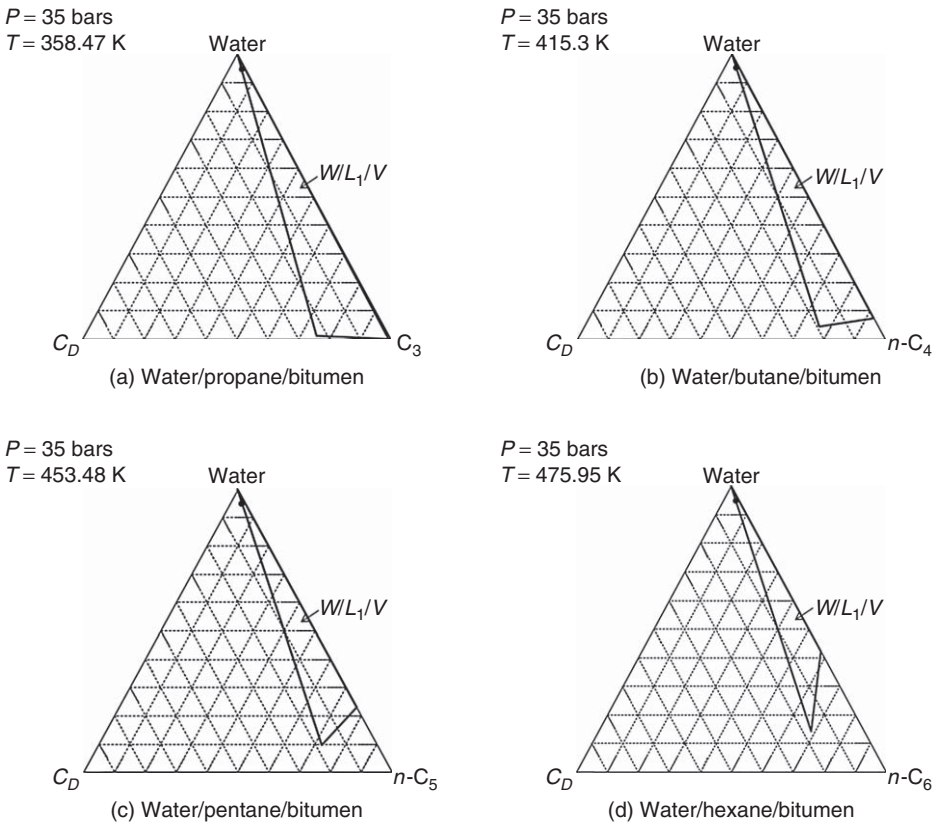

Fig. 4—Vapor-condensation temperatures at 35 bar for water/solvent/bitumen mixtures for a fixed overall composition of 95 mol% water, 4 mol% solvent, and 1 mol% bitumen (C_D). Four different alkane solvents are compared: propane, butane, pentane, and hexane. The overall composition is shown as the black dot on the *W*/*L* edge of the tie triangle for the aqueous (*W*), oleic (*L*), and vapor (*V*) phases. The PR EOS was used for the calculations (Tables 1 and 2). Two-phase regions associated with the tie triangle are omitted for clarity.

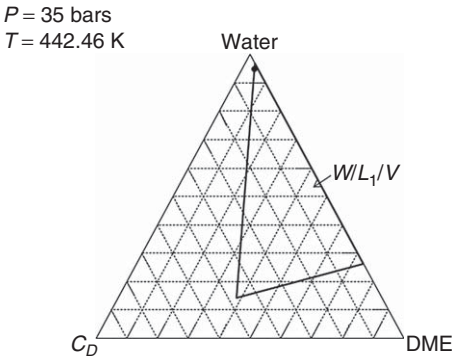

Fig. 5—Vapor-condensation temperature at 35 bar for the overall composition of 95 mol% water, 4 mol% DME, and 1 mol% bitumen (C_D). This overall composition is shown as the black dot on the *W*/*L* edge of the tie triangle for the aqueous (*W*), oleic (*L*), and vapor (*V*) phases. The PR EOS was used for the calculations. Two-phase regions associated with the tie triangle are omitted for clarity.

Fig. 6 shows liquid/liquid separation of bitumen/solvent mixtures in the presence of the W phase in the $W/L_1/L_2$ region. Such phase behavior was experimentally observed in Gao et al. (2017) for water/C_4/Athabasca-bitumen mixtures. Based on the experimental observation, they stated that the liquid/liquid separation would limit the solubility of solvent in bitumen even when a high level of solvent accumulation took place near the edge of a steam chamber in solvent-SAGD with highly volatile solvents. Fig. 6 shows that the upper-temperature limit for $W/L_1/L_2$ is calculated to be lower for the DME case than for the C_5 case. This indicates that the detrimental effect of $W/L_1/L_2$ phase behavior on bitumen dilution is less likely for DME-SAGD than for solvent-SAGD with solvents that are less volatile than DME, such as C_5; however, further investigation into bitumen dilution by DME is necessary with more experimental data.

Simulation Case Study

This section presents a simulation case study to compare SAGD, DME-SAGD, and C_4-SAGD. The comparison between SAGD and DME-SAGD is to see the effect of solvent on SAGD in terms of bitumen-production rate, CSOR, and ultimate oil recovery. The comparison between DME-SAGD and C_4-SAGD is to see the effect of the solubility of solvent in water on the previously discussed metrics

and solvent recovery. DME and C_4 are compared because of the similarity in terms of volatility (Fig. 3). Although the volatility of DME is closer to that of C_3 than C_4 (Fig. 3), C_3 is not selected in this case study because it does not improve SAGD for the bitumen reservoir considered here. The subsection Simulation Model describes the simulation conditions. Results are discussed in the subsection Simulation Results.

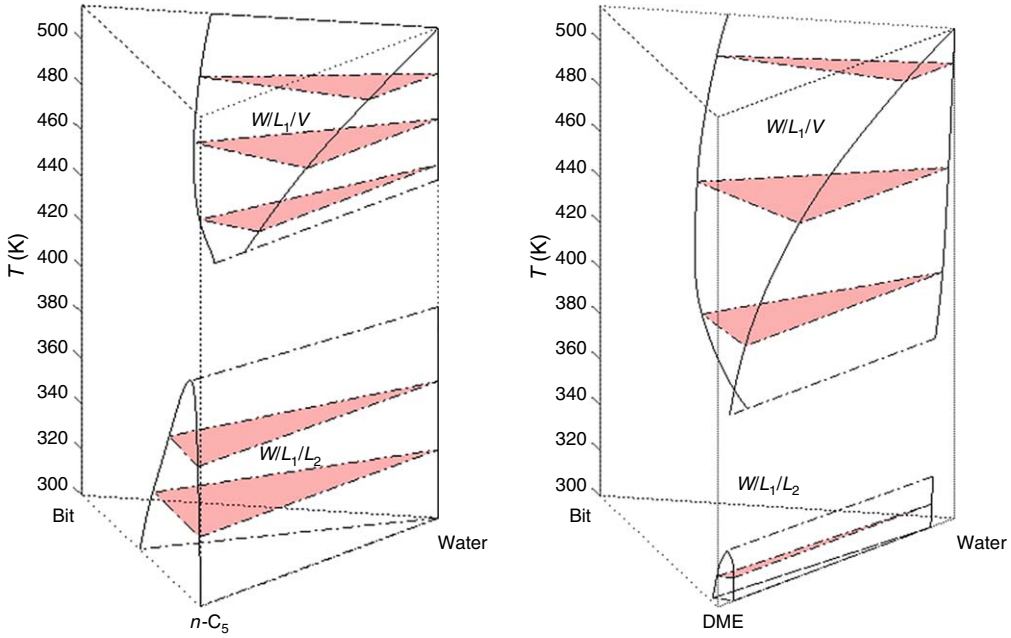

Fig. 6—Temperature/composition diagrams for water/solvent/bitumen at 35 bar using the PR-EOS model (Tables 1 and 2). Only three-phase regions are shown for clarity.

Simulation Model. With the STARS simulator (Computer Modelling Group 2014), one-half of a steam chamber is simulated for a homogeneous reservoir of 70 m (x) × 37.5 m (y) × 20 m (z). The reservoir is discretized into 70 × 1×20 gridblocks; that is, this is a vertical 2D model. The temperature and pressure of the initial reservoir are 15 bar and 286.15 K, respectively. The reservoir initially contains 25% water and 75% live bitumen with a gas/oil ratio of 0.44 m^3/m^3. The production well is placed at 3 m above the reservoir bottom, and the injection well is placed 4 m above the production well. The injection and production wells are operated at 35 and 15 bar, respectively. Other reservoir and well-pair parameters are summarized in **Table 3.**

Parameters	Values
Porosity	33%
Horizontal permeability	4,000 md
Vertical permeability	3,000 md
Initial reservoir pressure at the depth of 500 m	15 bar
Initial reservoir temperature	286.15 K
Initial oil saturation	0.75
Initial water saturation	0.25
Three-phase relative permeability model (CMG 2014)	Stone's Model II
Formation compressibility	1.8×10^{-3} 1/bar
Rock heat capacity (Keshavarz et al. 2014)	2600 kJ/(m^3·K)
Rock thermal conductivity (Keshavarz et al. 2014)	660 kJ/(m·d·K)
Over/underburden heat capacity (Keshavarz et al. 2014)	2600 kJ/(m^3·K)
Over/underburden thermal conductivity (Keshavarz et al. 2014)	660 kJ/(m·d·K)
Bitumen thermal conductivity	11.5 kJ/(m·d·K)
Gas thermal conductivity	2.89 kJ/(m·d·K)
Producer bottomhole pressure (minimum)	15 bar
Steam quality	0.9

Table 3—Input parameters for the simulation case study for SAGD and solvent-SAGD with the STARS simulator.

All simulations are conducted for 10 years of operation. The reservoir is first preheated for 6 months. Then, 2 mol% of solvent is coinjected with steam at 35 bar until the steam chamber reaches the side boundary of the reservoir model. After the coinjection period, 100% wet steam of 90% quality is injected until the end of the operation. This is because bitumen recovery gradually becomes less efficient, and solvent recovery becomes the focus in the final stage.

The viscosity model for water/*n*-alkane/bitumen is the same as those used in Venkatramani and Okuno (2016). That is, it takes into account the effect of water solubility in oil on *L*-phase viscosity. It also represents the difference between the mixing of water/bitumen and that of solvent/bitumen in terms of *L*-phase viscosity. Details of viscosities for water, *n*-alkanes, and bitumen as well as mixing coefficients for bitumen and *n*-alkanes can be found in their paper.

The correlation for viscosity of saturated-liquid DME by Wu et al. (2003) has been used to create a viscosity-temperature table at DME subcritical conditions for STARS. The correlation is

$$\log_{10}\mu = -5.7282 + \frac{631.031}{T} + 0.01453T - 1.8225\times10^{-5}T^2, \quad \ldots\ldots (3)$$

where μ is DME viscosity in cp and T is temperature in K. This correlation gives 0.5% AARD from experimental data measured from 227 to 343 K. DME is supercritical greater than 400.05 K (Table 1). To our knowledge, however, no data are available for viscosity of supercritical DME. Therefore, it is assumed to be the same as the supercritical viscosity of C_3 in this research. Coefficients in the viscosity-mixing rule for C_4 are used for DME in the absence of experimental viscosity data for bitumen/DME mixtures.

The STARS simulator models the *V*-phase densities by the ideal-gas law. The liquid phase densities can be calculated by the following mixing rule (no volume change on mixing):

$$1/\rho_j = \sum_{i=1}^{N_c} x_{ij}/\rho_{ij}, \quad \ldots\ldots (4)$$

where ρ_j is the molar density of liquid phase j, x_{ij} is the mole fraction of component i in liquid phase j, and N_C is the number of components. ρ_{ij} is the molar density of component i in phase j at T and P, which can be calculated as

$$\rho_{ij} = \rho_{i\,\mathrm{ref}}\exp\left[-\alpha_1(T-T_{\mathrm{ref}}) - \frac{1}{2}\alpha_2(T^2-T_{\mathrm{ref}}^2) + \alpha_3(P-P_{\mathrm{ref}}) + \alpha_4(P-P_{\mathrm{ref}})(T-T_{\mathrm{ref}})\right] \quad \ldots\ldots (5)$$

where P_{ref} is the reference pressure in kPa (101.325 kPa) and T_{ref} is the reference temperature in K (288.15 K). $\rho_{i\mathrm{ref}}$ is the molar density of component i at the reference pressure and temperature. The α-values are coefficients, and can be obtained together with $\rho_{i\mathrm{ref}}$ by regression to experimental data.

Densities for water, bitumen, and *n*-alkanes in this paper were taken by Venkatramani and Okuno (2016). Modified Rackett equations (Rackett 1970; Spencer and Danner 1972) were used by Ihmels and Lemmon (2007) for accurate representation of liquid DME density from 10 to 400 bar and 273 to 523 K. The liquid-density prediction from this model gives 0.039% AARD from experimental data. The modified Rackett equation is

$$\rho = \frac{\rho_0}{\{1 - C_T\ln[(B_T+P)/(B_T+P_0)]\}}, \quad \ldots\ldots (6)$$

where $\rho_0 = \dfrac{A_R}{B_R^{\left[1+\left(1-\frac{T}{C_R}\right)^{D_R}\right]}}$ and $B_T = B_{T_0} + B_{T_1}\dfrac{T}{E_T} + B_{T_2}\left(\dfrac{T}{E_T}\right)^2$. ρ is the liquid molar density of DME in mol/m^3. T and P are temperature and pressure in K and MPa, respectively. $C_T = 0.0834042$, $B_{T_0} = 284.304$ MPa, $B_{T_1} = -130.021$ MPa, $B_{T_2} = 14.4194$ MPa, $E_T = 100$ K, $A_R = 55.6001$ mol/m^3, $B_R = 0.236704$, $C_R = 401.406$ K, and $D_R = 0.243368$. The STARS simulator uses the liquid-density models described in Eqs. 4 and 5 instead of the Rackett equation. Therefore, Eqs. 4 and 5 were regressed to match predictions by the Rackett model up to 50 bar by adjusting the five parameters, $\rho_{i\mathrm{ref}}$, and α-values. The regression results give AAD and AARD of 14.9 kg/m^3 and 2.7%, respectively, and are given in **Tables 4 and 5** along with those coefficients for water, alkanes, and bitumen.

Component	ρ_{ref} (mol/m^3)	α_1 (K^{-1})	α_2 (K^{-2})	α_3 (kPa^{-1})	α_4 (kPa^{-1} K^{-1})
Water	55 425.9	-1.67×10^{-3}	6.48×10^{-6}	0.00	0.00
C_1	19 959.5	1.32×10^{-3}	5.77×10^{-6}	5.13×10^{-6}	4.05×10^{-8}
n-C_4	13 244.3	5.19×10^{-5}	5.05×10^{-6}	2.55×10^{-6}	4.56×10^{-9}
DME	15 682.7	2.95×10^{-4}	9.98×10^{-6}	4.02×10^{-6}	6.14×10^{-7}

Table 4—Density coefficients for the simulation case study with the STARS simulator. Values for water and *n*-alkanes were taken from Venkatramani and Okuno (2016). The α-values provided are for the use of Eq. 5 with the units of kPa and K as required by STARS.

System	ρ_{ref} (mol/m^3)	α_1 (K^{-1})	α_2 (K^{-2})	α_3 (kPa^{-1})	α_4 (kPa^{-1} K^{-1})
Water/*n*-C_4/C_D	1872.9	-2.23×10^{-5}	9.09×10^{-7}	3.88×10^{-7}	4.28×10^{-9}
Water/DME/C_D	1872.9	-1.95×10^{-5}	8.95×10^{-7}	3.85×10^{-7}	4.72×10^{-9}

Table 5—Bitumen density coefficients for STARS in the simulation case studies (Venkatramani and Okuno 2016). The α-values provided are for the use of Eq. 5 with the units of kPa and K as required by STARS.

The EOS models introduced in this section are used to generate *K*-value tables for phase-equilibrium calculation in the STARS simulator. In the tabulation of *K*-value tables, a possible solvent-rich liquid phase has been disregarded as required by the format of the STARS *K*-value tables. That is, the detrimental effect of liquid/liquid separation on bitumen dilution that can occur for C_4-SAGD is not simulated in this case study (see the preceding subsection Analysis of Vapor-Condensation Temperature at 35 bar and Fig. 6).

Simulation Results. ***Bitumen Recovery, CSOR, and Chamber-Edge Temperature.*** **Fig. 7** presents the cumulative bitumen-production histories simulated for SAGD, DME-SAGD, and C_4-SAGD. The bitumen-production rates of DME-SAGD are higher than SAGD. DME-SAGD yields 5% higher ultimate recovery of bitumen than SAGD because of the distillation mechanism (Keshavarz et al. 2014). For the same reason, C_4-SAGD is able to achieve a similar ultimate recovery to DME-SAGD. C_4-SAGD also shows the highest rate of bitumen production among the three processes studied here. Appendix A provides an explanation regarding the bitumen-drainage rate simulated for C_4-SAGD. The steam chamber reaches the side boundary at 3.8 years in DME-SAGD, 2.7 years in SAGD, and 2.9 years in C_4-SAGD. Therefore, steam/solvent coinjection is terminated at 3.8 years in DME-SAGD and 2.9 years in C_4-SAGD.

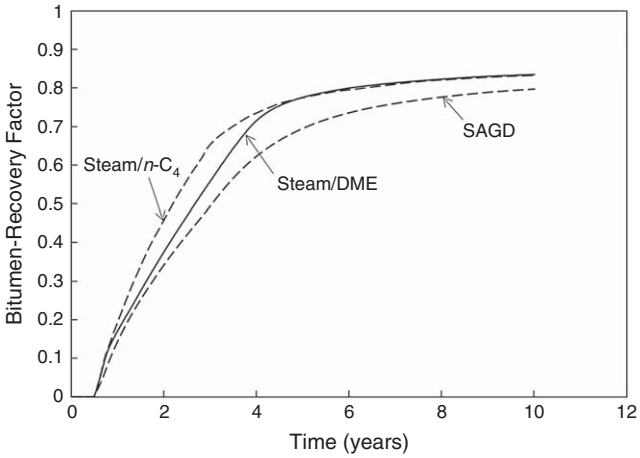

Fig. 7—Bitumen-recovery histories for steam/*n*-C_4, steam/DME, and SAGD simulations.

Fig. 8 shows the CSOR histories simulated for SAGD, DME-SAGD, and C_4-SAGD. DME-SAGD reduces CSOR by approximately 2 m^3/m^3 compared with SAGD, and C_4-SAGD reduces it even more in this case. The reduction in CSOR is because of the lower chamber temperature in solvent-SAGD (Keshavarz et al. 2015). **Fig. 9** shows the temperature profiles near the steam-chamber edge for the 12th row from the reservoir top for SAGD, DME-SAGD, and C_4-SAGD at 1.8 years. The chamber-edge temperature is 502 K for SAGD, 404 K for DME-SAGD, and 381 K for C_4-SAGD in Fig. 9. As expected from the analysis given previously, the chamber-edge temperature in DME-SAGD is simulated to be 23 K higher than that in C_4-SAGD, in spite of the higher volatility of DME compared with C_4 (Fig. 3).

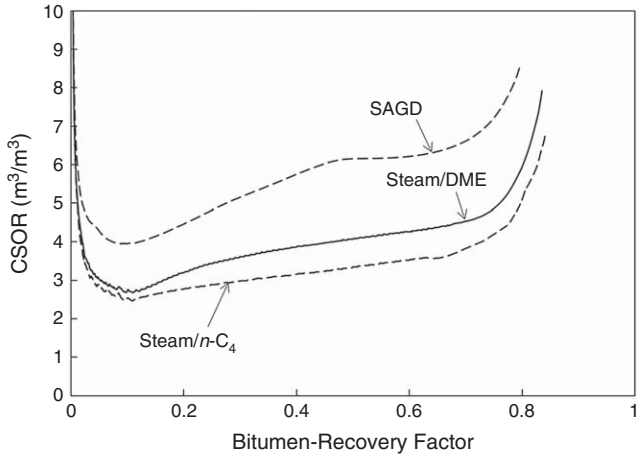

Fig. 8—CSOR for steam/*n*-C_4, steam/DME, and SAGD simulations.

Solvent Distribution in Phases and its Effects on Oil Recovery. **Fig. 10** shows the solvent mole fractions in the *L* and *W* phases for the 12th row from the reservoir top for DME-SAGD and C_4-SAGD. The DME concentration in the *W* phase is approximately 5 mol% within a few meters outside the chamber edge, which is consistent with Fig. 5. The *L* phase near the chamber edge contains approximately 90 mol% C_4 in C_4-SAGD, and a smaller amount of DME in DME-SAGD, as shown in Fig. 10a. This is qualitatively consistent with Figs. 4 and 5, in which the *L* phase contains less than 40 mol% DME in Fig. 5, but more than 75 mol% C_4 in Fig. 4 (vapor-condensation conditions for a fixed overall composition at 35 bar). In DME-SAGD, the dilution of bitumen by DME shown in Fig. 10a results in a SAGD-like bitumen-production rate (Fig. 7) while reducing SOR by 2 m^3/m^3, as shown in Fig. 8.

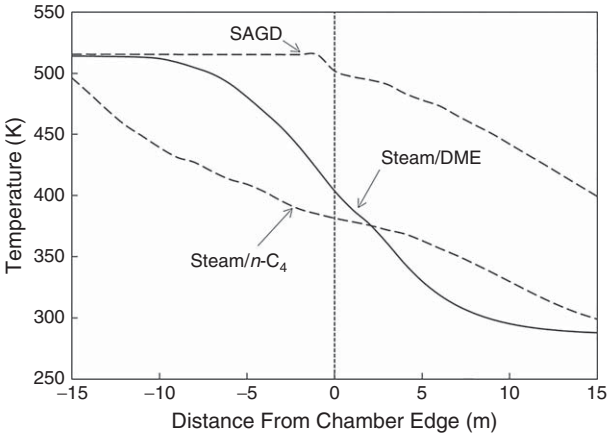

Fig. 9—Temperature profiles near the steam-chamber edge for the 12th row from the reservoir top at 1.8 years for steam/*n*-C_4, steam/DME, and SAGD simulations. The dashed line indicates the edge of a steam chamber, the left side of which is the steam chamber. Only the region within 15 m of the chamber edge is shown.

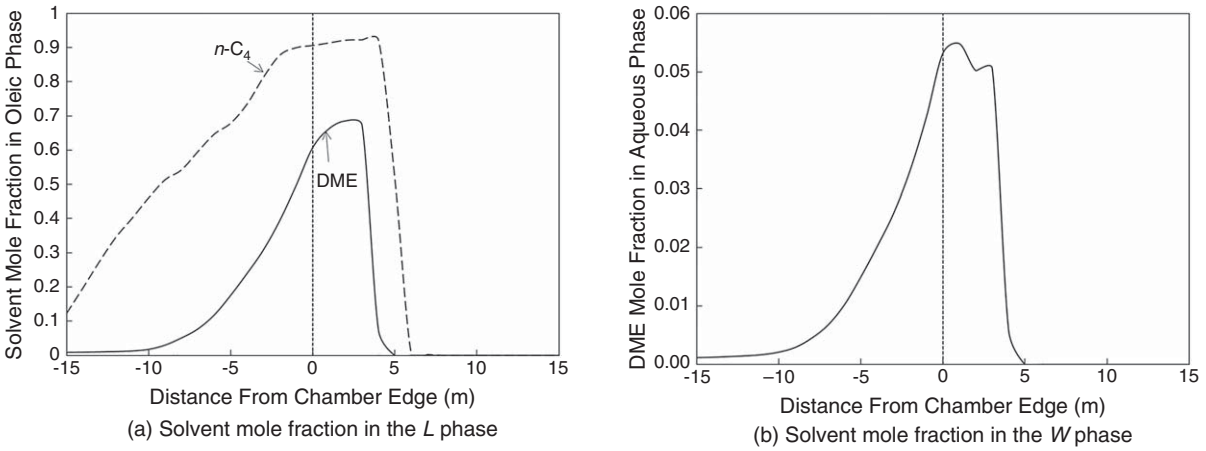

Fig. 10—Solvent mole fractions in the *L* and *W* phases for the 12th row from the reservoir top for DME-SAGD and C_4-SAGD simulations. The dashed line indicates the edge of a steam chamber, the left side of which is the steam chamber. Only the region within 15 m of the chamber edge is shown. (a) Solvent mole fraction in the *L* phase; (b) solvent mole fraction in the *W* phase.

The solubility of DME in water results in the distribution of DME among phases in DME-SAGD that is substantially different from that of C_4 in C_4-SAGD. **Fig. 11** presents the histories of solvent molar amounts in the *V, L,* and *W* phases for DME-SAGD and C_4-SAGD. In C_4-SAGD, a substantial amount of C_4 is present in the *V* phase, as is the case with solvent-SAGD using highly volatile solvents. At the moment the C_4 injection is terminated, approximately 50 mol% is in the *L* phase and 50 mol% is in the *V* phase. The solvent in the *V* phase decreases the in-situ temperature, which reduces heat losses to the overlying formation rocks and also facilitates the condensation of that solvent. However, the vapor solvent does not directly contribute to the dilution of bitumen. In DME-SAGD, the injected DME partitions into the *W, L,* and *V* phases inside the chamber and the *W* and *L* phases ahead of the chamber edge. Fig. 11 shows that approximately 47 mol% of the in-situ DME is in the *L* phase, 41 mol% in the *W* phase, and 12 mol% in the *V* phase upon the termination of solvent injection. That is, a substantial amount of DME resides in the *W* phase.

Fig. 12 shows the density distributions simulated for the *W* and *L* phases for DME-SAGD, C_4-SAGD, and SAGD for the 12th row from the reservoir top at 1.8 years. For DME-SAGD, the difference in mass density, $\Delta\rho_m$ (mass density of the *W* phase less mass density of the *L* phase), is close to zero in the gravity-drainage zone outside the steam chamber and negative inside the steam chamber, because of the partitioning of DME into the *W* and *L* phases. However, $\Delta\rho_m$ is simulated to be systematically negative in SAGD and positive in C_4-SAGD near the chamber edge. $\Delta\rho_m$ in the *L*/*W* two-phase flow along the chamber edge affects the compositional-flow regime, especially in solvent-SAGD.

Fig. 13 shows the molar flow rate of C_D in the *L* phase and that of water in the *W* phase in C_4-SAGD at 1.8 years. The chamber edge is indicated by black dots in Fig. 13. The transport of bitumen (C_D) clearly occurs above that of water because the *L* phase is less dense than the *W* phase in C_4-SAGD, as shown in Fig. 12 for the 12th row. **Fig. 14** shows the molar flow rate of C_D in the *L* phase and that of water in the *W* phase for DME-SAGD at 1.8 years. In DME-SAGD, the transport of C_D occurs more slowly, but in the thicker zone outside the chamber edge in comparison with C_4-SAGD (Figs. 13a and 14a). DME appears to have penetrated deeper outside the chamber edge because of the lower level of gravity segregation between the *L* and *W* phases in DME-SAGD. This can be clearly seen in **Fig. 15,** which shows the maps for the overall mole fraction of C_4 in C_4-SAGD and that of DME in DME-SAGD at 1.8 years. **Fig. 16** presents the profiles of overall composition for DME-SAGD, C_4-SAGD, and SAGD at the 12th row from the reservoir top at 1.8 years. The overall concentration of DME is higher outside the chamber than inside the chamber in DME-SAGD. This is in contrast to the C_4-concentration profile shown in Fig. 16b for C_4-SAGD. In C_4-SAGD, a substantial amount of C_4 is used to transport a small amount of bitumen (C_D) (approximately 1 mol% in Fig. 16a), which makes a C_4 bank flowing with the *W* phase with a large positive $\Delta\rho_m$. In DME-SAGD, a larger amount of C_D is diluted by a smaller amount of solvent, and the segregation of the *L* and *W* phases is less clear (Fig. 16a, b).

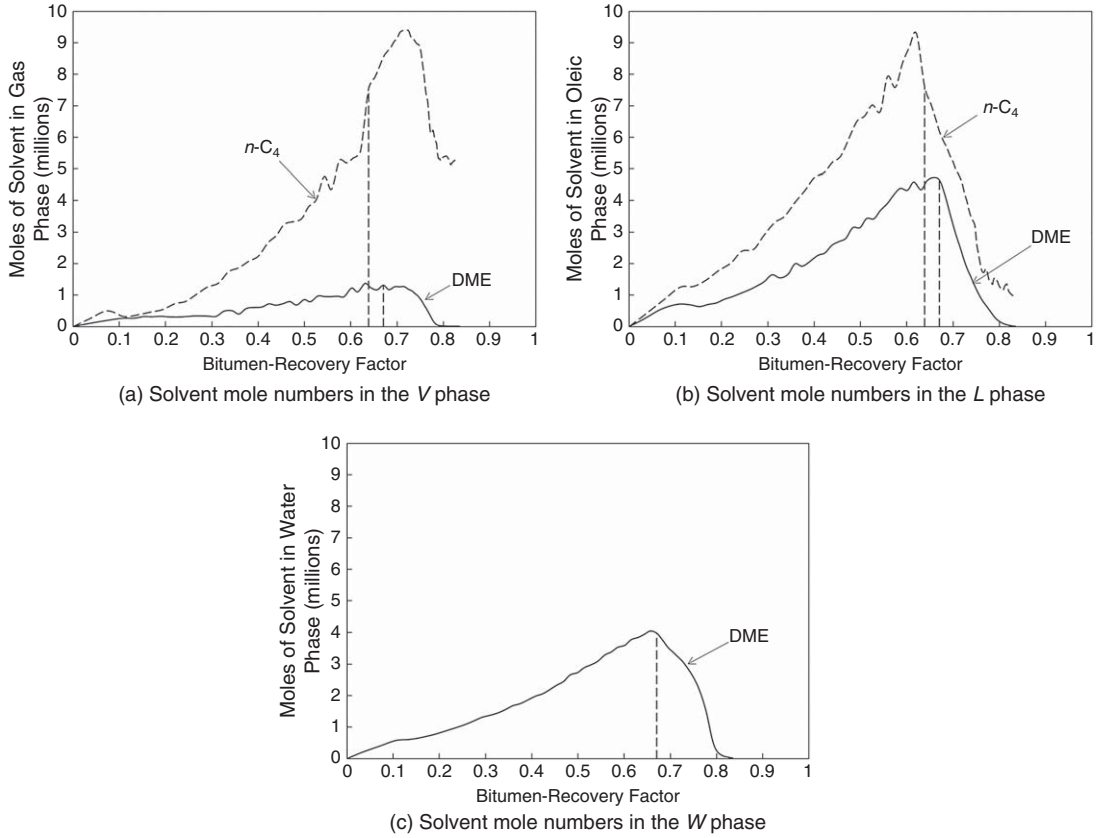

Fig. 11—Histories of solvent mole numbers in the *V*, *L*, and *W* phases for DME-SAGD and C_4-SAGD simulations. The dashed line indicates when the solvent injection is terminated. (a) Solvent mole numbers in the *V* phase; (b) solvent mole numbers in the *L* phase; (c) solvent mole numbers in the *W* phase.

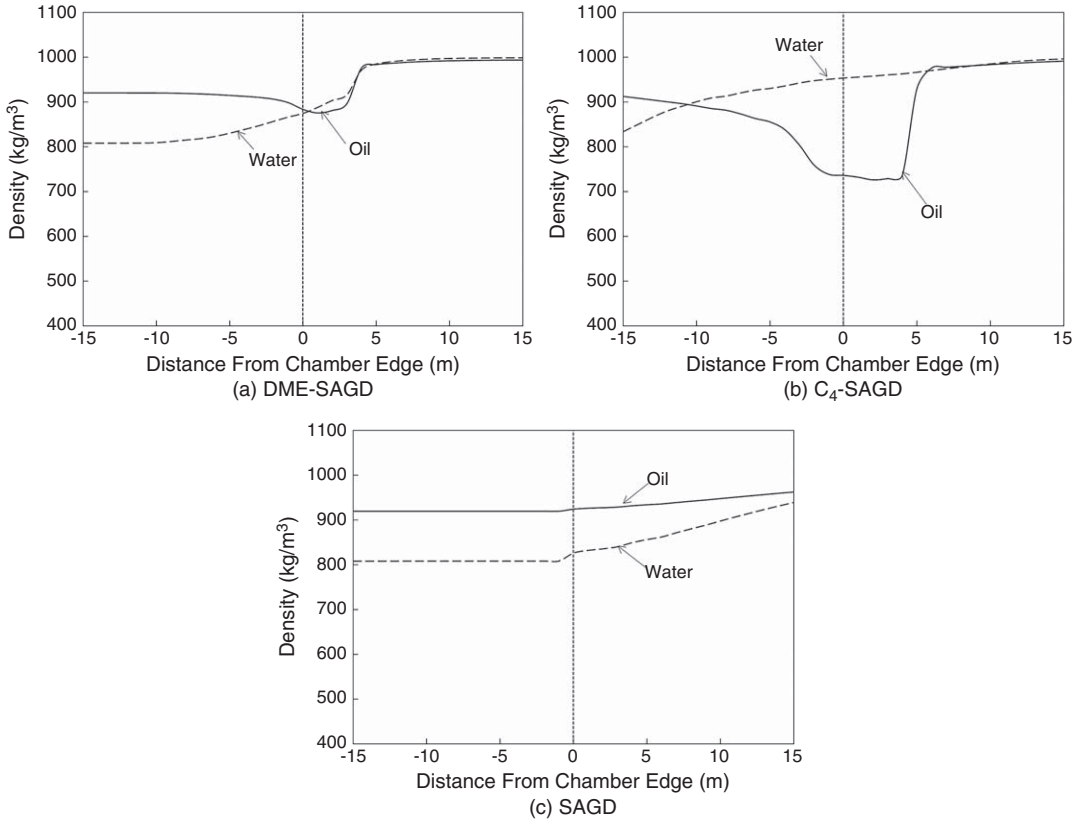

Fig. 12—Density distributions simulated for the *W* and *L* phases for DME-SAGD, C_4-SAGD, and SAGD for the 12th row from the reservoir top at 1.8 years. The dashed line indicates the edge of a steam chamber, the left side of which is the steam chamber. Only the region within 15 m of the chamber edge is shown. (a) DME-SAGD; (b) C_4-SAGD; (c) SAGD.

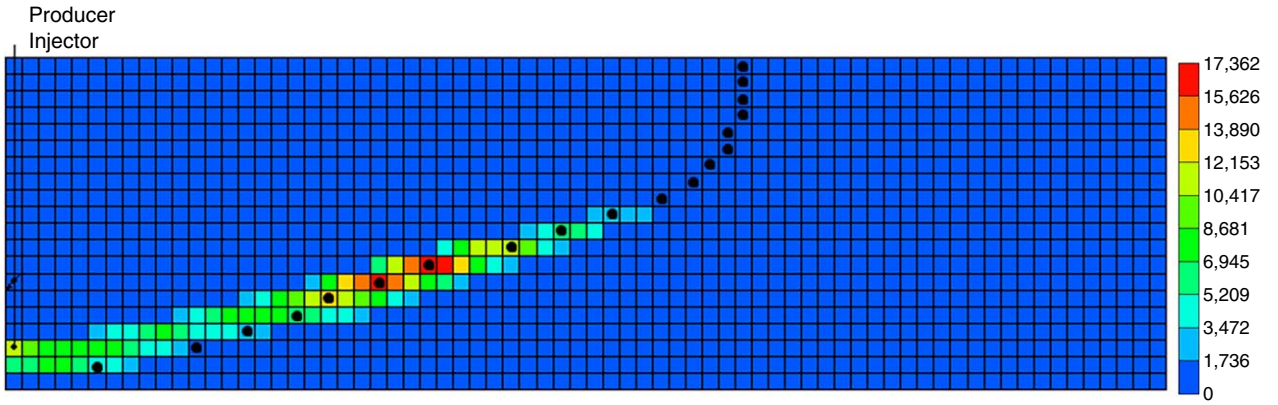

(a) Molar flow rate of C_D in the *L* phase

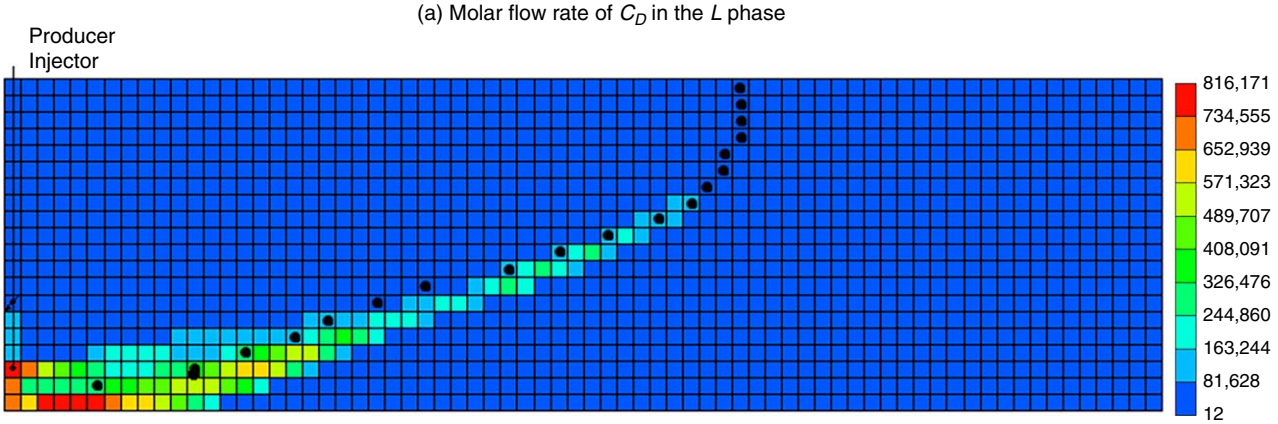

(b) Molar flow rate of water in the *W* phase

Fig. 13—2D maps for (a) molar flow rate of the bitumen component (C_D) in the *L* phase (mol/D), and (b) molar flow rate of water in the *W* phase (mol/D) in C_4-SAGD at 1.8 years. The chamber edge is indicated by black dots.

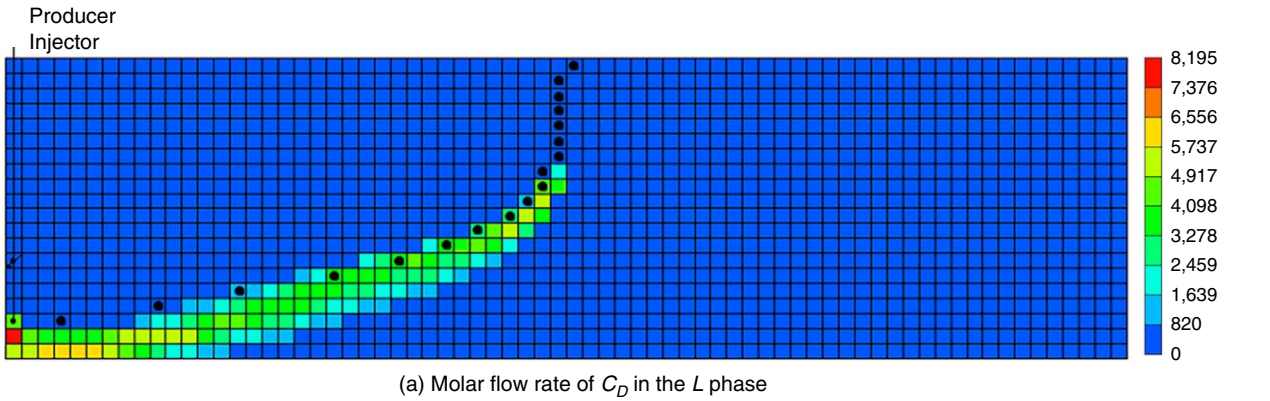

(a) Molar flow rate of C_D in the *L* phase

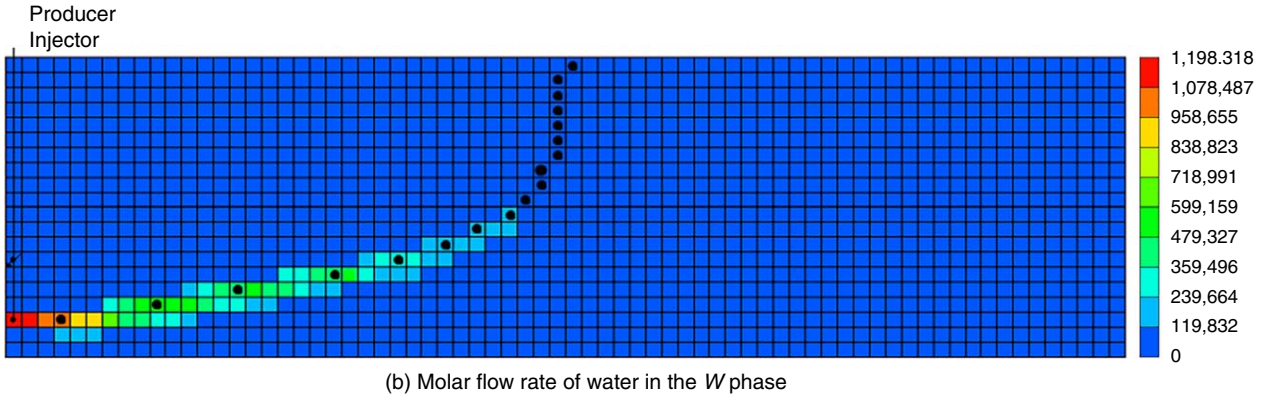

(b) Molar flow rate of water in the *W* phase

Fig. 14—2D maps for (a) molar flow rate of the bitumen component (C_D) in the *L* phase (mol/D), and (b) molar flow rate of water in the *W* phase (mol/D) in DME-SAGD at 1.8 years. The chamber edge is indicated by black dots.

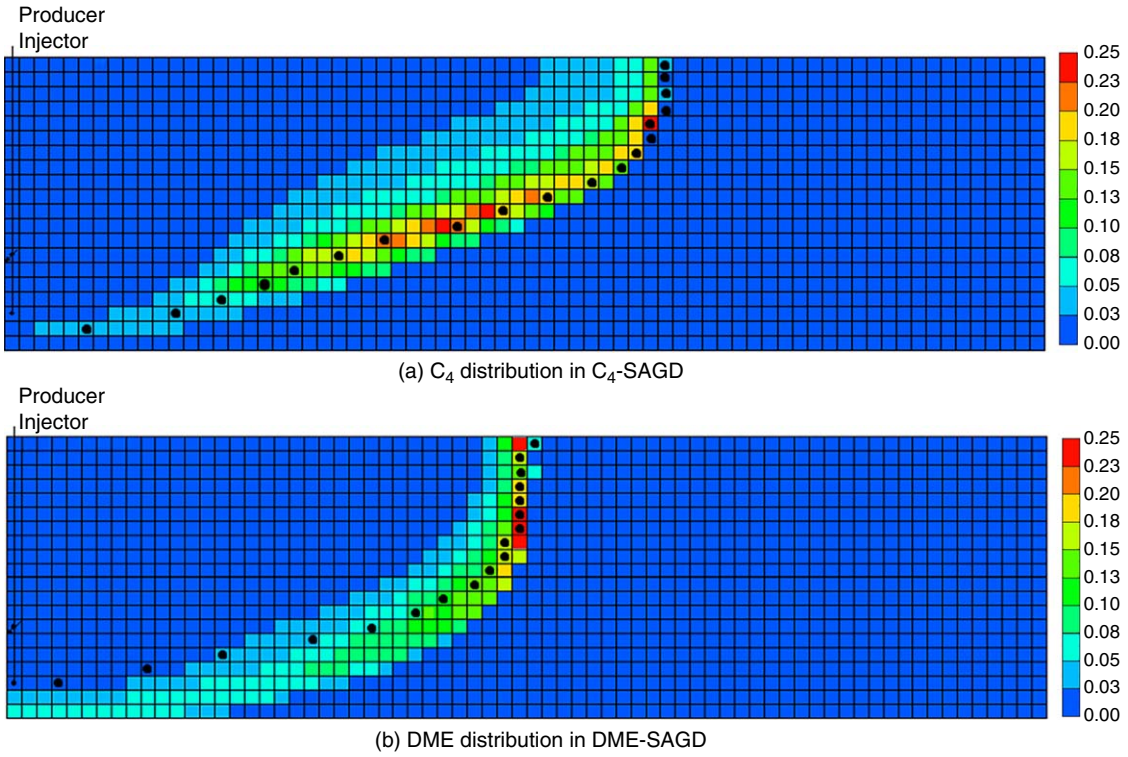

Fig. 15—Overall concentration of C_4 in C_4-SAGD and that of DME in DME-SAGD at 1.8 years. The chamber edge is indicated by black dots. (a) C_4 distribution in C_4-SAGD; (b) DME distribution in DME-SAGD.

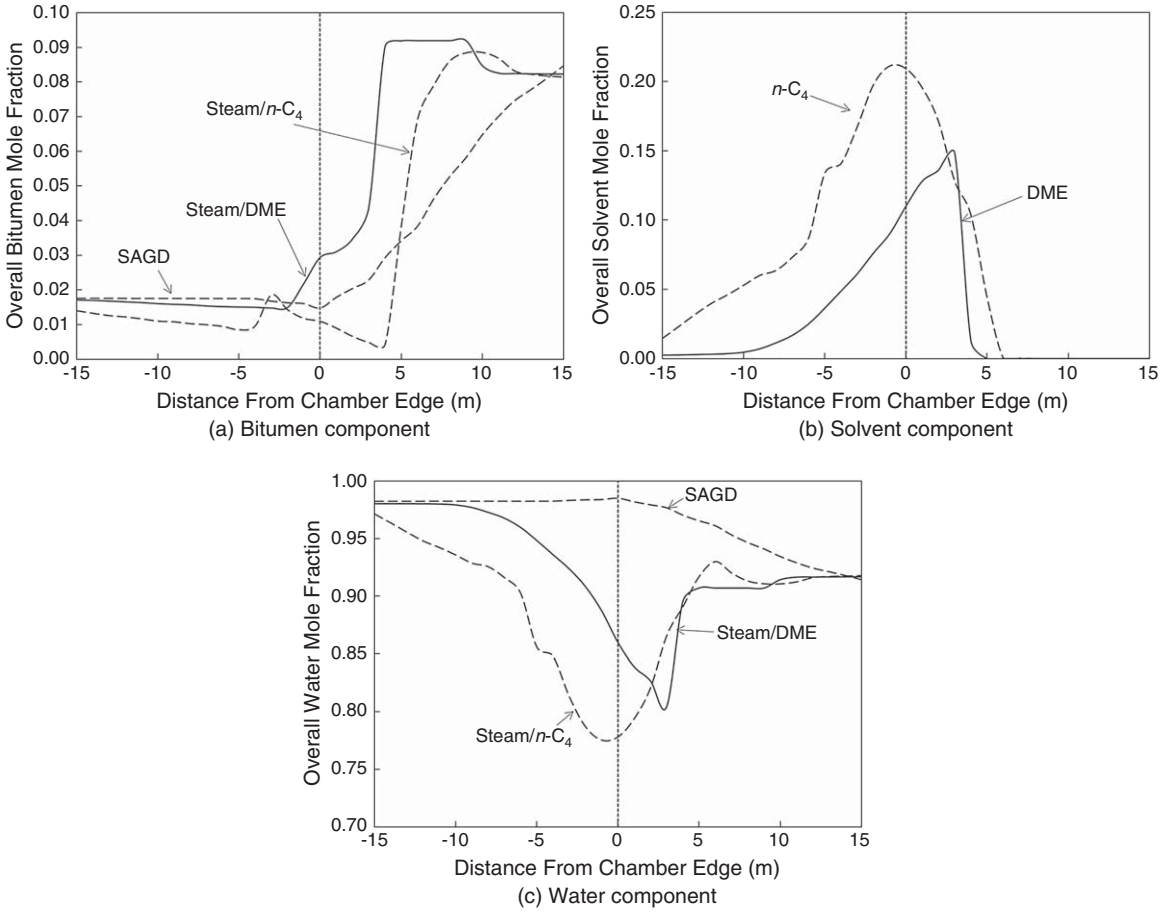

Fig. 16—Profiles of overall composition for DME-SAGD, C_4-SAGD, and SAGD at the 12th row from the reservoir top at 1.8 years. The dashed line indicates the edge of a steam chamber, the left side of which is the steam chamber. Only the region within 15 m of the chamber edge is shown. (a) Bitumen component; (b) solvent component; (c) water component.

Mechanical mixing in the L phase occurs mainly between solvent and bitumen in C_4-SAGD and DME-SAGD. It also occurs between solvent and water in the W phase in DME-SAGD because of the partitioning of DME in the W phase. It is known that such mechanical mixing in porous media requires convective fluid flow. Fig. 13 shows that the mixing of C_4 with bitumen is expected in the L phase flowing above the flowing W phase. Fig. 14 shows that the mixing of DME with bitumen is expected within a greater volume mostly outside of the chamber edge, with a smaller level of gravity segregation between the L and W phases.

The DME distribution among phases given in Fig. 11 also improves solvent recovery in DME-SAGD compared with C_4-SAGD. **Fig. 17** shows that the solvent recovery factor in DME-SAGD is systematically higher than that of C_4-SAGD (approximately by 15%). The solvent recovery factor is defined here as the cumulative volume of solvent produced divided by the cumulative volume of solvent injected at a given time. In DME-SAGD, 89% of DME is recovered by the produced W phase, and 11% from the produced L phase measured at the reservoir conditions. In C_4-SAGD, 100% of C_4 is from the produced L phases because C_4 is insoluble in water.

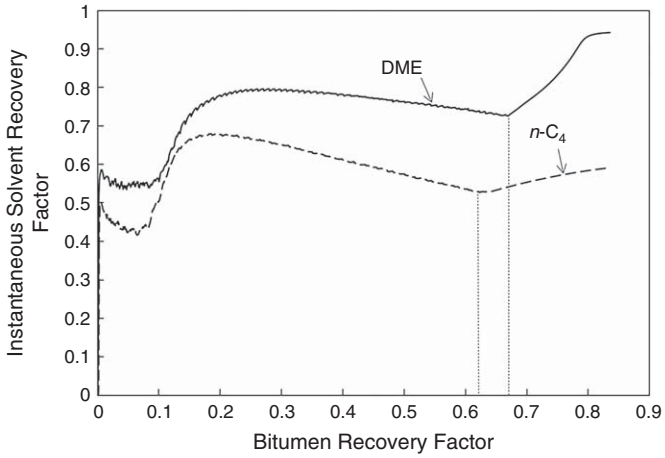

Fig. 17—Solvent recovery factor for DME-SAGD and C_4-SAGD. The recovery factor is defined here as the cumulative volume of solvent produced divided by the cumulative volume of solvent injected at a given time. The vertical line indicates when the solvent injection is terminated.

One of the main uncertainties in the model is the L-phase viscosity for DME-SAGD as mentioned in the Simulation Case Study section. Appendix B presents a sensitivity analysis regarding the effects of the viscosity model and the number of gridblocks on simulation results.

Conclusions

This paper was concerned primarily with the potential of DME, a water-soluble solvent, as an additive to steam for improving the efficiency of SAGD. The secondary objective of this paper was to investigate how the solubility of DME in water affects solvent-SAGD. DME and Athabasca bitumen were considered as the water-soluble solvent and bitumen, respectively, in this study. However, it is beyond the scope of this research to single out a particular compound as a promising water-soluble additive to steam for a given bitumen/heavy oil. Conclusions are as follows:

1. Although DME is more volatile than C_4, the solubility of DME in water in DME-SAGD results in chamber-edge temperatures that are higher than those in C_4-SAGD. This can be explained by ternary phase behavior of water/solvent/bitumen mixtures; that is, the transition from *WLV* to *WL* for such a system tends to occur at a higher temperature for a given overall composition and pressure when the solvent partitions into the W phase.
2. The solubility of DME in bitumen is nearly one-half that of C_4 at their corresponding chamber-edge conditions (Figs. 4, 5, and 10). In DME-SAGD simulations, however, approximately 47 mol% of the in-situ DME was used for dilution of bitumen, which was equivalent to the fraction of the in-situ C_4 used for bitumen dilution in C_4-SAGD. This occurs likely because the partitioning of DME into bitumen and water reduces the gravity segregation of the two-liquid-phase flow along the edge of a steam chamber in DME-SAGD. The reduced gravity segregation in DME-SAGD is expected to facilitate the mixing of condensed DME with bitumen. This is in contrast to C_4-SAGD, in which the L phase diluted by a substantial amount of C_4 is much less dense than the W phase, impeding the contact between the C_4 bank and bitumen along the edge of a steam chamber.
3. Simulation results showed that the vapor fraction of the in-situ solvent was much smaller in DME-SAGD than in C_4-SAGD. Also, the injected DME can be recovered not only by the L phase, but also by the W phase in DME-SAGD. Therefore, the recovery factor of solvent was simulated to be systematically higher (by approximately 15%) in DME-SAGD than in C_4-SAGD.
4. Simulation results showed that DME-SAGD yielded 35% reduction in SOR in comparison with SAGD while being able to keep SAGD-like rates of bitumen production. DME-SAGD also resulted in 5% higher ultimate recovery of bitumen than SAGD. However, C_4-SAGD was simulated to be superior to DME-SAGD in terms of bitumen-production rate and SOR in the case studied.

Nomenclature

$A, B, C, D,$ and E = coefficients in the modified Rackett equation (Rackett 1970; Spencer and Danner 1972)
g = gravitational constant, 9.8 m/s^2
k = permeability
L = oleic phase
P = pressure
Q = molar flow rate, mol/s

S = saturation
T = temperature, K
V = vapor phase
$\underline{V}$ = molar volume, cm^3/mol
W = aqueous phase
x = mole fraction
y = length of reservoir parallel to well pair, m
α = density coefficient
θ = angle between tangent to chamber edge and horizontal line
μ = dynamic viscosity, mPa·s
ξ = distance from perpendicular to chamber edge, m
ρ = molar density, mol/m^3
ν = kinematic viscosity, $cp \cdot m^3/kg$
ω = acentric factor

Subscripts

bit = bitumen
c = critical condition
C_D = dead bitumen
HC = hydrocarbon
L = oleic phase
ref = reference condition
sol = solvent
V = vapor phase
w = water

Acknowledgments

We gratefully acknowledge the financial support from Japan Petroleum Exploration Company Limited and Japan Canada Oil Sands Limited. Okuno holds the Pioneer Corporation Faculty Fellowship in Petroleum Engineering at the University of Texas at Austin.

References

Alkindi, A., Al-Azri, N., Said, D. et al. 2016. Persistence in EOR—Design of a Field Trial in a Carbonate Reservoir Using Solvent-Based Water-Flood Process. Presented at the SPE EOR Conference at Oil and Gas West Asia, Muscat, Oman, 21–23 March. SPE-179838-MS. https://doi.org/10.2118/179838-MS.

Amani, M. J., Gray, M. R., and Shaw, J. M. 2013a. Phase Behavior of Athabasca Bitumen + Water Mixtures at High Temperature and Pressure. *J. Supercrit. Fluids* **77** (May): 142–152. https://doi.org/10.1016/j.supflu.2013.03.007.

Amani, M. J., Gray, M. R., and Shaw, J. M. 2013b. Volume of Mixing and Solubility of Water in Athabasca Bitumen at High Temperature and Pressure. *Fluid Phase Equilibr.* **358** (25 November): 203–211. https://doi.org/10.1016/j.fluid.2013.07.021.

American Petroleum Institute (API). 1983. *API Technical Data Book: Petroleum Refining*, fourth edition. New York City: American Petroleum Institute.

Baek, K. H., Sheng, K., Argüelles-Vivas, F. J. et al. 2017. Comparative Study of Oil-Dilution Capability of Dimethyl Ether (DME) and Hexane as Steam Additives for SAGD. Presented at the SPE Annual Technical Conference and Exhibition, San Antonio, Texas, 9–11 October. SPE-187182-MS. https://doi.org/10.2118/187182-MS.

Brunner, E. 1990. Fluid Mixtures at High Pressures IX. Phase Separation and Critical Phenomena in 23 (*n*-alkane + water) Mixtures. *J. Chem. Thermodyn.* **22** (4): 335–353. https://doi.org/10.1016/0021-9614(90)90120-F.

Butler, R. M. 1997. *Thermal Recovery of Oil and Bitumen*. Calgary: GravDrain, Inc.

Chahardowli, M., Farajzadeh, R., and Bruining, H. 2016. Experimental Investigation of Dimethyl Ether/Polymer Hybrid as an Enhanced Oil Recovery Method. Presented at the SPE EOR Conference at Oil and Gas West Asia, Muscat, Oman, 21–23 March. SPE-179850-MS. https://doi.org/10.2118/179850-MS.

Chapman, W. G., Gubbins, K. E., Joslin, C. G. et al. 1986. Theory and Simulation of Associating Liquid Mixtures. *Fluid Phase Equilibr.* **29** (October): 337–346. https://doi.org/10.1016/0378-3812(86)85033-6.

Chernetsky, A., Masalmeh, S., Eikmans, D. et al. 2015. A Novel Enhanced Oil Recovery Technique: Experimental Results and Modelling Workflow of the DME Enhanced Waterflood Technology. Presented at the Abu Dhabi International Petroleum Exhibition and Conference, Abu Dhabi, 9–12 November. SPE-177919-MS. https://doi.org/10.2118/177919-MS.

Computer Modelling Group (CMG). 2014. *STARS Version 2014 User's Guide*. Calgary: CMG.

Constantinou, L. and Gani. R. 1994. New Group Contribution Method for Estimating Properties of Pure Compounds. *AIChE J.* **40** (10): 1697–1710. https://doi.org/10.1002/aic.690401011.

Constantinou, L., Gani, R., and O'Connell, J. P. 1995. Estimation of the Acentric Factor and the Liquid Molar Volume at 298 K Using a New Group Contribution Method. *Fluid Phase Equilibr.* **103** (1): 11–22. https://doi.org/10.1016/0378-3812(94)02593-P.

Folas, G. K., Kontogeorgis, G. M., Michelsen, M. L. et al. 2006a. Application of the Cubic-Plus Association Equation of State to Mixtures with Polar Chemicals and High Pressures. *Ind. Eng. Chem. Res.* **45** (4): 1516–1526. https://doi.org/10.1021/ie0509241.

Folas, G. K., Kontogeorgis, G. M., Michelsen, M. L. et al. 2006b. Application of the Cubic-Plus-Association (CPA) Equation of State to Complex Mixtures with Aromatic Hydrocarbons. *Ind. Eng. Chem. Res.* **45** (4): 1527–1538. https://doi.org/10.1021/ie050976q.

Ganjdanesh, R., Rezaveisi, M., Pope, G. A. et al. 2016. Treatment of Condensate and Water Blocks in Hydraulic-Fractured Shale-Gas/Condensate Reservoirs. *SPE J.* **21** (2): 665–674. SPE-175145-PA. https://doi.org/10.2118/175145-PA.

Gao, J., Okuno, R., and Li, H. A. 2017. An Experimental Study of Multiphase Behavior for *n*-Butane/Bitumen/Water Mixtures. *SPE J.* **22** (3):783–798. SPE-180736-PA. https://doi.org/10.2118/180736-PA.

Gates, I. D. 2007. Oil Phase Viscosity Behavior in Expanding-Solvent Steam-Assisted Gravity Drainage. *J. Pet. Sci. Eng.* **59** (1–2): 123–134. https://doi.org/10.1016/j.petrol.2007.03.006.

Groot, J. A. W. M., Chernetsky, A., Te Riele, P. M. et al. 2016a. Representation of Phase Behavior and PVT Workflow for DME Enhanced Water-Flooding. Presented at the SPE EOR Conference at Oil and Gas West Asia, Muscat, Oman, 21–23 March. SPE-179771-MS. https://doi.org/10.2118/179771-MS.

Groot, J. A. W. M., Eikmans, D., Fadili, A. et al. 2016b. Field-Scale Modeling and Sensitivity Analysis of DME Enhanced Waterflooding. Presented at SPE EOR Conference at Oil and Gas West Asia, Muscat, Oman, 21–23 March. SPE-179798-MS. https://doi.org/10.2118/179798-MS.

Gupta, S. C. and Gittins, S. D. 2006. Christina Lake Solvent Aided Process Pilot. *J Can Pet Technol* **45** (9): 15–18. PETSOC-06-09-TN. https://doi.org/10.2118/06-09-TN.

Gupta, S., Gittins, S., and Picherack, P. 2005. Field Implementation of Solvent Aided Process. *J Can Pet Technol* **44** (11): 8–13. PETSOC-05-11-TN1. https://doi.org/10.2118/05-11-TN1.

Holldorff, H. and Knapp, H. 1988. Binary Vapor-Liquid-Liquid Equilibrium of Dimethyl Ether—Water and Mutual Solubilities of Methyl Chloride and Water. *Fluid Phase Equilibr.* **44** (2): 195–209. https://doi.org/10.1016/0378-3812(88)80111-0.

Huron, M. J. and Vidal, J. 1979. New Mixing Rules in Simple Equations of State for Representing Vapour-Liquid Equilibria of Strongly Non-ideal Mixtures. *Fluid Phase Equilibr.* **3** (4): 255–271. https://doi.org/10.1016/0378-3812(79)80001-1.

Ihmels, E. C. and Lemmon, E. W. 2007. Experimental Densities, Vapor Pressures, and Critical Point, and a Fundamental Equation of State for Dimethyl Ether. *Fluid Phase Equilibr.* **260** (1): 36–48. https://doi.org/10.1016/j.fluid.2006.09.016.

Ivory, J. J., Zheng, R., Nasr, T. N. et al. 2008. Investigation of Low Pressure ES-SAGD. Presented at International Thermal Operations and Heavy Oil Symposium, Calgary, 20–23 October. SPE-117759-MS. https://doi.org/10.2118/117759-MS.

Keshavarz, M., Okuno, R., and Babadagli, T. 2014. Efficient Oil Displacement Near the Chamber Edge in ES-SAGD. *J. Pet. Sci. Eng.* **118** (June): 99–113. https://doi.org/10.1016/j.petrol.2014.04.007.

Keshavarz, M., Okuno, R., and Babadagli, T. 2015. Optimal Application Conditions for Steam/Solvent Coinjection. *SPE Res Eval & Eng* **18** (1): 20–38. SPE-165471-PA. https://doi.org/10.2118/165471-PA.

Kontogeorgis, G. M. and Folas, G. K. 2009. *Thermodynamic Models for Industrial Applications: From Classical and Advanced Mixing Rules to Association Theories*. Hoboken, New Jersey: John Wiley & Sons.

Kontogeorgis, G. M., Voutsas, E. C., Yakoumis, I. V. et al. 1996. An Equation of State for Associating Fluids. *Ind. Eng. Chem. Res.* **35** (11): 4310–4318. https://doi.org/10.1021/ie9600203.

Kumar, A. 2016. *Characterization of Reservoir Fluids Based on Perturbation from* n-*Alkanes*. PhD dissertation, University of Alberta, Edmonton, Alberta, Canada.

Kumar, A. and Okuno, R. 2016. Reliable Characterization of Bitumen Based on Perturbation from *n*-alkanes for Steam-Solvent Coinjection Simulation. *Fuel* **182** (15 October): 141–153. https://doi.org/10.1016/j.fuel.2016.05.095.

Leaute, R. P. 2002. Liquid Addition to Steam for Enhancing Recovery (LASER) of Bitumen With CSS: Evolution of Technology From Research Concept to a Field Pilot at Cold Lake. Presented at the SPE International Thermal Operations and Heavy Oil Symposium and International Horizontal Well Technology Conference, Calgary, 4–7 November. SPE-79011-MS. https://doi.org/10.2118/79011-MS.

Leaute, R. P. and Carey, B. S. 2007. Liquid Addition to Steam for Enhancing Recovery (LASER) of Bitumen With CSS: Results From the First Pilot Cycle. *J Can Pet Technol* **46** (9): 22–30. PETSOC-07-09-01. https://doi.org/10.2118/07-09-01.

Li, W., Mamora, D. D., and Li, Y. 2011a. Light- and Heavy-Solvent Impacts on Solvent-Aided-SAGD Process: A Low-Pressure Experimental Study. *J Can Pet Technol* **50** (4): 19–30. SPE-133277-PA. https://doi.org/10.2118/133277-PA.

Li, W., Mamora, D. D., and Li, Y. 2011b. Solvent-Type and -Ratio Impacts on Solvent-Aided SAGD Process. *SPE Res Eval & Eng* **14** (3): 320–331. SPE-130802-PA. https://doi.org/10.2118/130802-PA.

Michelsen, M. L. 1990. A Modified Huron-Vidal Mixing Rule for Cubic Equations of State. *Fluid Phase Equilibr.* **60** (1–2): 213–219. https://doi.org/10.1016/0378-3812(90)85053-D.

Mohebati, M. H., Maini, B. B., and Harding, T. G. 2012. Numerical-Simulation Investigation of the Effect of Heavy-Oil Viscosity on the Performance of Hydrocarbon Additives in SAGD. *SPE Res Eval & Eng* **15** (2): 165–181. SPE-138151-PA. https://doi.org/10.2118/138151-PA.

Nasr, T. N., Beaulieu, G., Golbeck, H. et al. 2003. Novel Expanding Solvent-SAGD Process "ES-SAGD". *J Can Pet Technol* **42** (1): 13–16. PETSOC-03-01-TN. https://doi.org/10.2118/03-01-TN.

Oliveira, M. B., Coutinho, J. A. P., and Queimada, A. J. 2007. Mutual Solubilities of Hydrocarbons and Water With the CPA EoS, *Fluid Phase Equilibr.* **258** (1): 58–66. https://doi.org/10.1016/j.fluid.2007.05.023.

Park, K.-J., Seo, T., and Jung, D. 2007. Performance of Alternative Refrigerants for Residential Air-Conditioning Applications. *Appl. Energ.* **84** (10): 985–991. https://doi.org/10.1016/j.apenergy.2007.05.002.

Parsons, C., Chernetsky, A., Eikmans, D. et al. 2016. Introducing a Novel Enhanced Oil Recovery Technology. Presented at the SPE Improved Oil Recovery Conference, Tulsa, 11–13 April. SPE-179560-MS. https://doi.org/10.2118/179560-MS.

Pedersen, K. S., Christensen, P. L., and Shaikh, J. A. 2014. *Phase Behavior of Petroleum Reservoir Fluids*. Boca Raton, Florida: CRC Press.

Pozo, M. E. and Streett, W. B. 1984. Fluid Phase Equilibria for the System Dimethyl Ether/Water from 50 to 220 C and Pressures to 50.9 MPa. *J. Chem. Eng. Data* **29** (3): 324–329. https://doi.org/10.1021/je00037a030.

Rackett, H. G. 1970. Equation of State for Saturated Liquids. *J. Chem. Eng. Data* **15** (4): 514–517. https://doi.org/10.1021/je60047a012.

Ratnakar, R. R., Dindoruk, B., and Wilson, L. 2016a. Experimental Investigation of DME-Water-Crude Oil Phase Behavior and PVT Modeling for the Application of DME-Enhanced Waterflooding. *Fuel* **182** (15 October): 188–197. https://doi.org/10.1016/j.fuel.2016.05.096.

Ratnakar, R. R., Dindoruk, B., and Wilson, L. 2016b. Phase Behavior Experiments and PVT Modeling of DME-Brine-Crude Oil Mixtures Based on Huron-Vidal Mixing Rules for EOR Applications. *Fluid Phase Equilibr.* **434** (25 February): 49–62. https://doi.org/10.1016/j.fluid.2016.11.021.

Reamer, H. H., Sage, B. H., and Lacey, W. N. 1952. Phase Equilibria in Hydrocarbon Systems. *n*-Butane-Water System in the Two-Phase Region. *Ind. Eng. Chem.* **44** (3): 609–615. https://doi.org/10.1021/ie50507a049.

Riazi, M. R. and Daubert, T. E. 1987. Characterization Parameters for Petroleum Fractions. *Ind. Eng. Chem. Res.* **26** (4): 755–759. https://doi.org/10.1021/ie00064a023.

Robinson, D. B. and Peng, D. Y. 1978. The Characterization of the Heptanes and Heavier Fractions for the GPA Peng-Robinson Programs. Research Report RR-28, Gas Processors Association, Tulsa.

Scharlin, P., Battino, R., Silla, E. et al. 1998. Solubility of Gases in Water: Correlation Between Solubility and the Number of Water Molecules in the First Solvation Shell. *Pure Appl. Chem.* **70** (10): 1895–1904. https://doi.org/10.1351/pac199870101895.

Shen, C. 2013. *Enhanced Oil Recovery: Field Case Studies*, first edition. Elsevier.

Shi, X. 2016. *Analytical Solution for SAGD With Consideration of Temperature Variation Along the Edge of a Steam Chamber*. Master's thesis, University of Alberta, Edmonton, Alberta, Canada, December 2016.

Shi, X. and Okuno, R. 2018. Analytical Solution for Steam-Assisted Gravity Drainage With Consideration of Temperature Variation Along the Edge of a Steam Chamber. *Fuel* **217:** 262–274. https://doi.org/10.1016/j.fuel.2017.12.110.

Soave, G. 1972. Equilibrium Constants From a Modified Redlich-Kwong Equation of State. *Chem. Eng. Sci.* **27** (6): 1197–1203. https://doi.org/10.1016/0009-2509(72)80096-4.

Spencer, C. F. and Danner, R. P. 1972. Improved Equation for Prediction of Saturated Liquid Density. *J. Chem. Eng. Data* **17** (2): 236–241. https://doi.org/10.1021/je60053a012.
Tallon, S. and Fenton, K. 2010. The Solubility of Water in Mixtures of Dimethyl Ether and Carbon Dioxide. *Fluid Phase Equilibr.* **298** (1): 60–66. https://doi.org/10.1016/j.fluid.2010.07.009.
Te Riele, P., Parsons, C., Boerrigter, P. et al. 2016. Implementing a Water Soluble Solvent Based Enhanced Oil Recovery Technology—Aspects of Field Development Planning. Presented at the SPE EOR Conference at Oil and Gas West Asia, Muscat, Oman, 21–23 March. SPE-179849-MS. https://doi.org/10.2118/179849-MS.
Venkatramani, A. V. and Okuno, R. 2015. Characterization of Water-Containing Reservoir Oil Using an EOS for Steam Injection Processes. *J. Nat. Gas Sci. Eng.* **26** (September): 1091–1106. https://doi.org/10.1016/j.jngse.2015.07.036.
Venkatramani, A. V. and Okuno, R. 2016. Compositional Mechanisms in Steam-Assisted Gravity Drainage and Expanding-Solvent Steam-Assisted Gravity Drainage With Consideration of Water Solubility in Oil. *SPE Res Eval & Eng* **20** (3): 681–697. SPE-180737-PA. https://doi.org/10.2118/180737-PA.
Venkatramani, A. V. and Okuno, R. 2017. Steam-Solvent Coinjection Under Reservoir Heterogeneity: Should ES-SAGD be Implemented for Highly Heterogeneous Reservoirs? Presented at the SPE Canada Heavy Oil Technical Conference, Calgary, 15–16 February. SPE-185001-MS. https://doi.org/10.2118/185001-MS.
Wu, J. and Yin, J. 2008. Vapor Pressure Measurements of Dimethyl Ether From (213 to 393) K. *J. Chem. Eng. Data* **53** (9): 2247–2249. https://doi.org/10.1021/je800375t.
Wu, J., Liu, Z., Bi, S. et al. 2003. Viscosity of Saturated Liquid Dimethyl Ether from (227 to 343) K. *J. Chem. Eng. Data* **48** (2): 426–429. https://doi.org/10.1021/je0256232.
Wu, J., Liu, Z., Wang, B. et al. 2004. Measurement of the Critical Parameters and the Saturation Densities of Dimethyl Ether. *J. Chem. Eng. Data* **49** (3): 704–708. https://doi.org/10.1021/je034251+.
Zhu, D. and Okuno, R. 2016. Multiphase Isenthalpic Flash Integrated With Stability Analysis. *Fluid Phase Equilibr.* **423** (15 September): 203–219. https://doi.org/10.1016/j.fluid.2016.04.005.

Appendix A—Explanation of C_4-SAGD Performance Given in the Subsection Simulation Results

In the subsection Simulation Results, the C_4-SAGD case resulted in higher bitumen-drainage rates than the DME-SAGD case before the steam chamber reached the reservoir boundary (Fig. 7). It was also simulated that the solvent's distribution ahead of the steam-chamber edge was substantially different between the C_4-SAGD and DME-SAGD cases (Figs. 10, 15, and 16) because these cases resulted in different levels of gravity segregation between the *W* and *L* phases. This appendix provides a more-detailed explanation of how the solvent distribution affects bitumen molar flow ahead of the edge of a steam chamber (Figs. 13 and 14).

Following the derivation of Butler (1997), Shi (2016), and Shi and Okuno (2018), Darcy's flow velocity for the *L* phase is integrated for a cross section perpendicular to the edge of a steam chamber to give the following expression for molar flow rate of bitumen Q_{bit} at elevation z:

$$Q_{\mathrm{bit}}(z) = \int_0^{\xi_L} u_L \rho_L x_{\mathrm{bit}L} \Delta y \mathrm{d}\xi = -kg\sin\theta\Delta y \int_0^{\xi_L} \frac{k_{rL}}{\nu_L} \rho_L x_{\mathrm{bit}L} \mathrm{d}\xi, \qquad \text{(A-1)}$$

where u_L is Darcy's flow velocity for the L phase, ρ_L is molar density of the *L* phase, $x_{\mathrm{bit}L}$ is bitumen mole fraction in the *L* phase, ξ_L is the thickness of mobilized oil perpendicular to the steam chamber edge, Δy is the horizontal-section length, k is the absolute permeability, g is gravitational acceleration, θ is the angle between the chamber edge and horizontal line at elevation z, k_{rL} is the *L*-phase relative permeability, and ν_L is kinematic viscosity of the *L* phase. Eq. A-1 indicates that molar flow rate of bitumen is affected by the profiles of *L*-phase saturation, kinematic viscosity, molar density, and bitumen concentration.

To confirm the simulation results given in the subsection Simulation Results, Eq. A-1 was applied to the C_4-SAGD and DME-SAGD cases. **Fig. A-1** compares the profiles of the integrand in Eq. A-1 in log scale [i.e., $\log_{10}\left(\frac{k_{rL}}{\nu_L}\rho_L x_{\mathrm{bit}L}\right)$] for C_4-SAGD and DME-SAGD at 1.8 years. Then, a discretized form of Eq. A-1 was applied to compare the bitumen molar flow rates evaluated for the perpendicular line originated at elevation of 10 m on the corresponding chamber edge. It was confirmed that the molar flow rate of bitumen for C_4-SAGD was calculated to be approximately 1.2 times that of DME-SAGD using Eq. A-1 for the midelevation, $z = 10$ m.

Analysis of Fig. A-1 using Eq. A-1 has indicated that the greater molar flow of bitumen in C_4-SAGD occurs mainly because *L*-phase kinematic viscosity is substantially low, but *L*-phase molar volume is high where *L*-phase relative permeability is high in the vicinity of the chamber edge. Although the *L*-phase bitumen concentration is low near the chamber edge, the bitumen molar flow in C_4-SAGD is simulated to be greater than that in DME-SAGD because the effect of substantially low kinematic viscosity is amplified by the high molar density and relative permeability near the chamber edge $\left(\text{i.e.,} \frac{k_{rL}}{\nu_L}\rho_L\right)$.

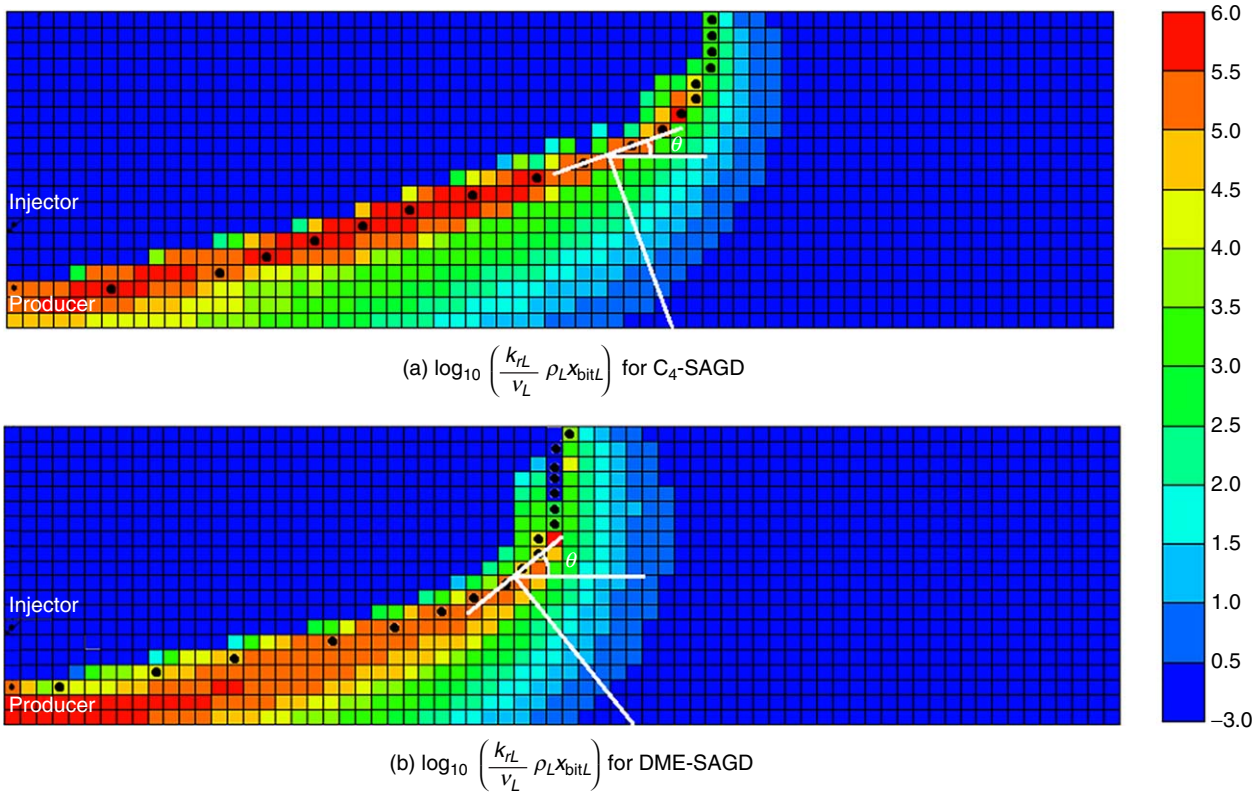

(a) $\log_{10}\left(\frac{k_{rL}}{\nu_L}\rho_L x_{\text{bit}L}\right)$ for C_4-SAGD

(b) $\log_{10}\left(\frac{k_{rL}}{\nu_L}\rho_L x_{\text{bit}L}\right)$ for DME-SAGD

Fig. A-1—2D map of $\log_{10}\left(\frac{k_{rL}}{\nu_L}\rho_L x_{\text{bit}L}\right)$ at 1.8 years. The unit for $\left(\frac{k_{rL}}{\nu_L}\rho_L x_{\text{bit}L}\right)$ is (kg·mol·cp^{-1}·m^{-6}). Black dots indicate the edge of a steam chamber. White solid lines indicate tangents and normal lines at 10 m from the top of the reservoir. θ is the angle between the tangent line and horizontal line. (a) $\log_{10}\left(\frac{k_{rL}}{\nu_L}\rho_L x_{\text{bit}L}\right)$ for C_4-SAGD; (b) $\log_{10}\left(\frac{k_{rL}}{\nu_L}\rho_L x_{\text{bit}L}\right)$ for DME-SAGD.

Appendix B—Sensitivity Analysis

This appendix shows sensitivity analysis of simulation results in terms of the viscosity model used for the L phase and the number of gridblocks.

Viscosity Model. As mentioned in the subsection Simulation Model, the viscosity model for the L phase containing DME is currently uncertain in the literature. In the section Simulation Case Study, the same coefficients for the nonlinear log mixing rule were used for both C_4-SAGD and DME-SAGD, considering the similarity of DME and C_4 in terms of volatility.

The mixing rule for L-phase viscosity in STARS is

$$\ln\mu_L = \sum_{i=1}^{N_c} q_i x_{iL} \ln\mu_{iL} = \sum_{i=1}^{N_c} f_i \ln\mu_{iL}, \quad \text{(B-1)}$$

subject to $\sum_{i=1}^{N_c} q_i x_{iL} = \sum_{i=1}^{N_c} f_i = 1.0$. Bitumen is set as the key component, and its weighting factor can be calculated as follows (Venkatramani and Okuno 2016):

$$q_{CD} = 1 + \alpha\left\{\frac{(1-x_{CDL})[1-(1-x_{CDL})^8]}{x_{CDL}}\right\}, \quad \text{(B-2)}$$

where α is a constant specific to the solvent used. Weighting factors for the other components are set to be identical subject to Eq. B-1. In the section Simulation Case Study, the α-value used for C_4-SAGD and DME-SAGD is 0.43.

Figs. B-1 and B-2 show simulation results when α is set to 0.20 for DME-SAGD. Compared with 0.43, the α-value of 0.20 results in better agreement with the data recently measured for Athabasca-bitumen/DME mixtures at different temperatures at 35 bar (Baek et al. 2017). With this viscosity model, the drainage rate of DME-SAGD with α of 0.20 is simulated to be approximately 10% greater than that with α of 0.43. Accordingly, the cumulative SOR of DME-SAGD to recover the same amount of bitumen is lowered by approximately 0.5 m^3/m^3. The instantaneous recovery of DME is simulated to be approximately 5% higher. The density difference between the L and W phases near the chamber edge in DME-SAGD at 1.8 years remains small compared with that of C_4-SAGD.

Number of Gridblocks. Simulations of C_4-SAGD, DME-SAGD, and SAGD were repeated with four times more gridblocks ($140 \times 1 \times 40$) under the same conditions as the section Simulation Case Study. However, nonconvergence was observed for these fine-scale simulations. **Fig. B-3** shows bitumen-recovery curves before the simulation was terminated because of nonconvergence. Bitumen-drainage rates for C_4-SAGD, DME-SAGD, and SAGD were simulated to be higher than the original cases (section Simulation Case Study). However, relative positions of bitumen-recovery curves in those three fine-grid cases are similar to those for the coarse-grid cases in the section Simulation Case Study. It is unlikely that the number of gridblocks used affects the conclusions of the current research, as explained here.

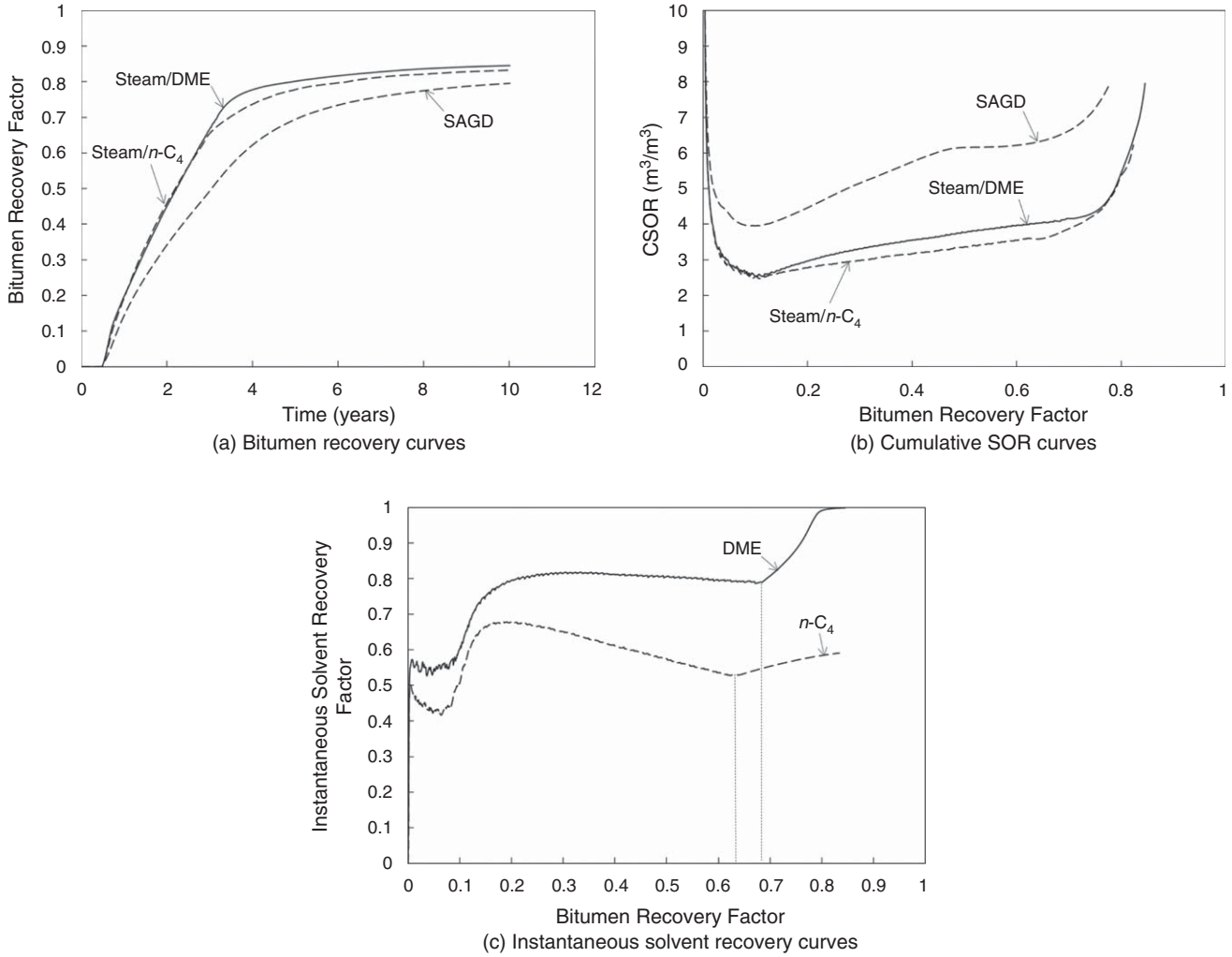

Fig. B-1—Comparisons of bitumen recovery, SOR, and solvent recovery among C_4-SAGD, SAGD, and DME-SAGD with the viscosity parameter α of 0.20. This value of α is dependent on the data recently measured for mixtures of Athabasca bitumen with DME (Baek et al. 2017). (a) Bitumen-recovery curves; (b) CSOR curves; (c) instantaneous-solvent-recovery curves.

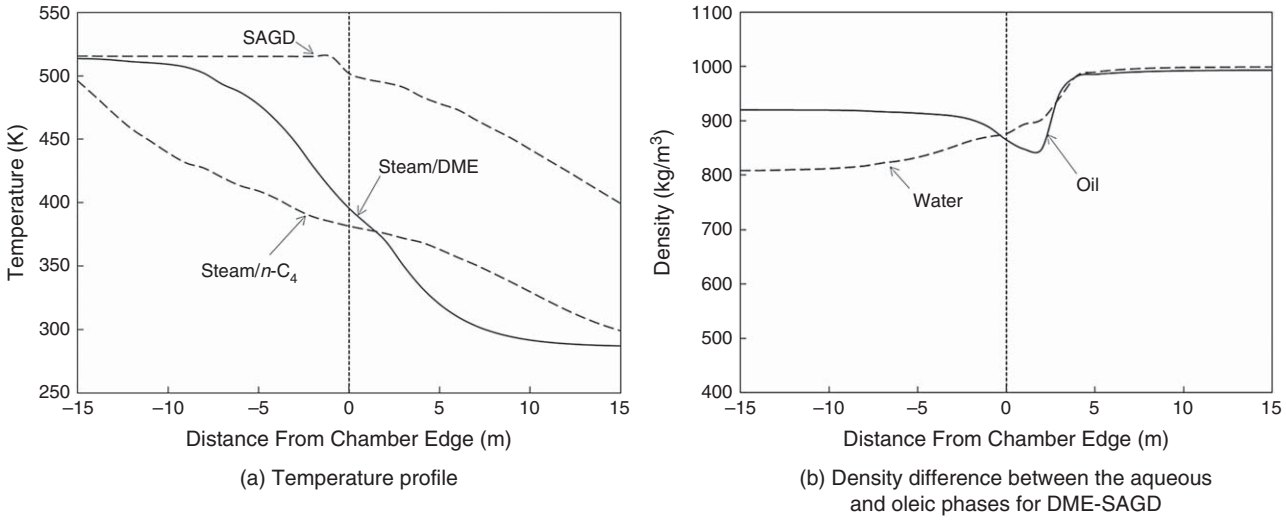

Fig. B-2—Profiles of temperature and phase densities for C_4-SAGD, DME-SAGD, and SAGD at the 12th row from the reservoir top at 1.8 years. DME-SAGD in this figure used the viscosity parameter $\alpha = 0.20$. Only the region within 15 m of the chamber edge is shown. (a) Temperature profile; (b) density difference between the aqueous and oleic phases for DME-SAGD.

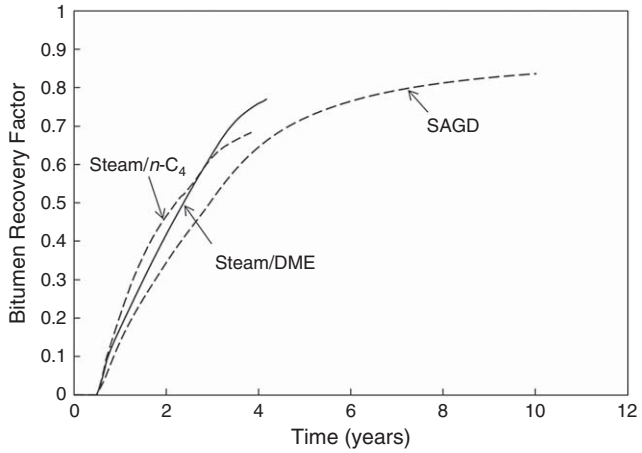

Fig. B-3—Bitumen-recovery curves for SAGD, C_4-SAGD, and DME-SAGD when four times more gridblocks are used. All cases show greater bitumen-drainage rates during the first several years compared with the coarse-grid cases presented in the section Simulation Case Study. Relative positions of their bitumen-recovery curves remain the same (see Fig. 7).

Fig. B-4 shows the temperature distribution near the chamber edge at the 24th row from the reservoir top at 1.8 years for each SAGD process. In Fig. B-4, simulated chamber-edge temperatures for C_4-SAGD, DME-SAGD, and SAGD cases are 382, 402 and 508 K, respectively. That is, the difference in simulated chamber-edge temperature between the fine- and coarse-gridding cases is 1 K for C_4-SAGD, 2 K for DME-SAGD, and 6 K for SAGD (see the section Simulation Case Study and Fig. 9).

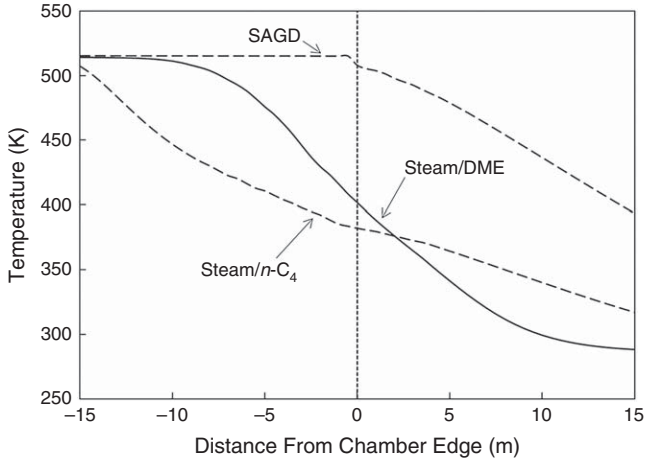

Fig. B-4—Profiles of temperature for C_4-SAGD, DME-SAGD, and SAGD at the 24th row from the reservoir top at 1.8 years when four times more gridblocks are used. The vertical line indicates the edge of a steam chamber, the left side of which is the steam chamber. Only the region within 15 m of the chamber edge is shown.

Fig. B-5 shows profiles of oil and water densities near the chamber edge at the 24th row from the reservoir top at 1.8 years. Observations from Fig. B-5 are similar to those from Fig. 12; that is, the water phase is much denser than the oil phase in C_4-SAGD, but the opposite is observed in SAGD near the chamber edge. In DME-SAGD, the density difference between the two liquid phases is much smaller.

Fig. B-6 shows profiles of water, bitumen, and solvent near the chamber edge at the 24th row from the reservoir top at 1.8 years. The highest concentration of C_4 appears slightly inside the steam-chamber edge, and the highest concentration of DME appears outside of the chamber edge. In the region where the highest concentration of DME appears, there is higher concentration of bitumen. Similar observations were made from Fig. 16 using a coarser gridding.

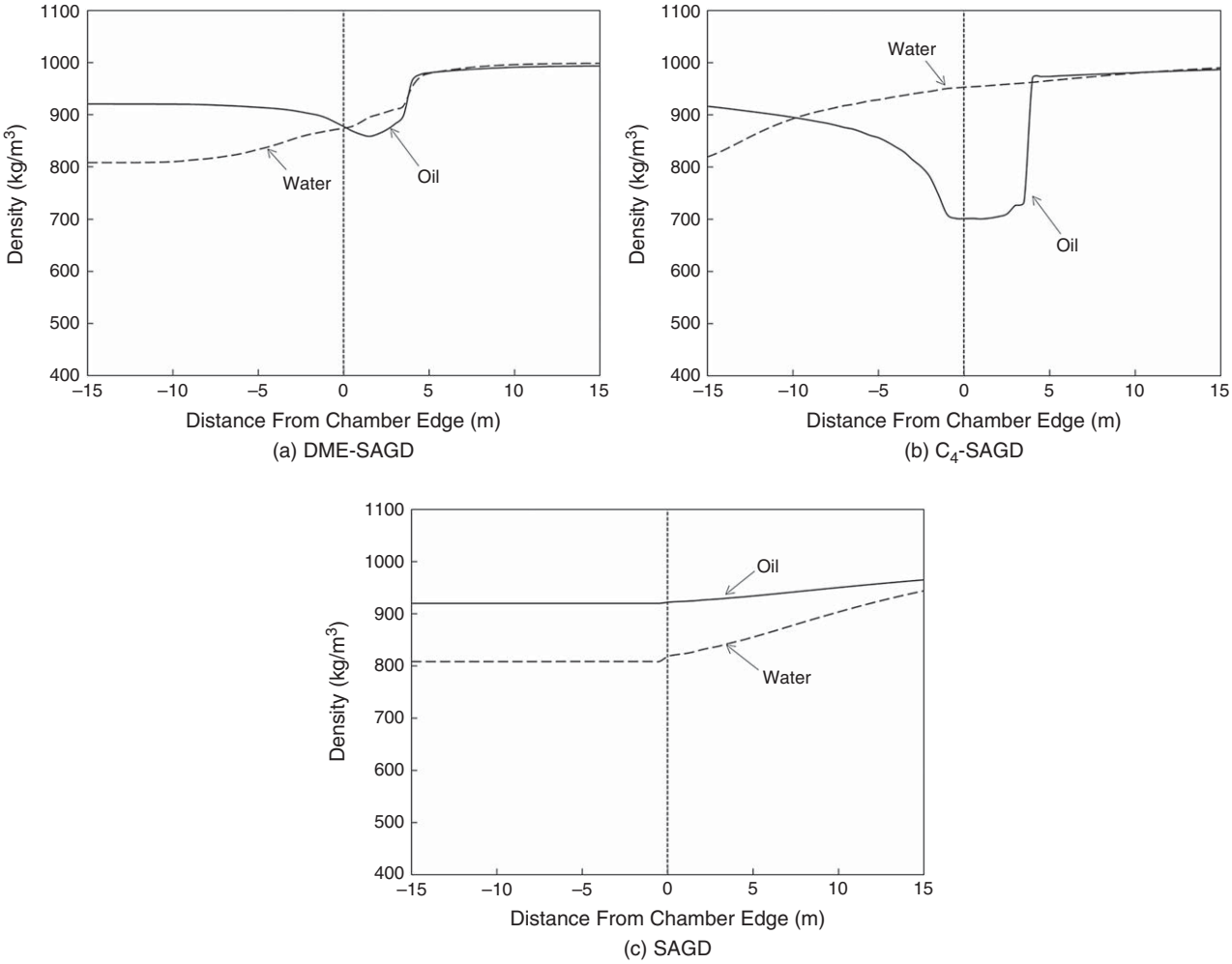

Fig. B-5—Profiles of phase densities for C_4-SAGD, DME-SAGD, and SAGD at the 24th row from the reservoir top at 1.8 years when four times more gridblocks are used. The vertical line indicates the edge of a steam chamber, the left side of which is the steam chamber. Only the region within 15 m of the chamber edge is shown. (a) DME-SAGD; (b) C_4-SAGD; (c) SAGD.

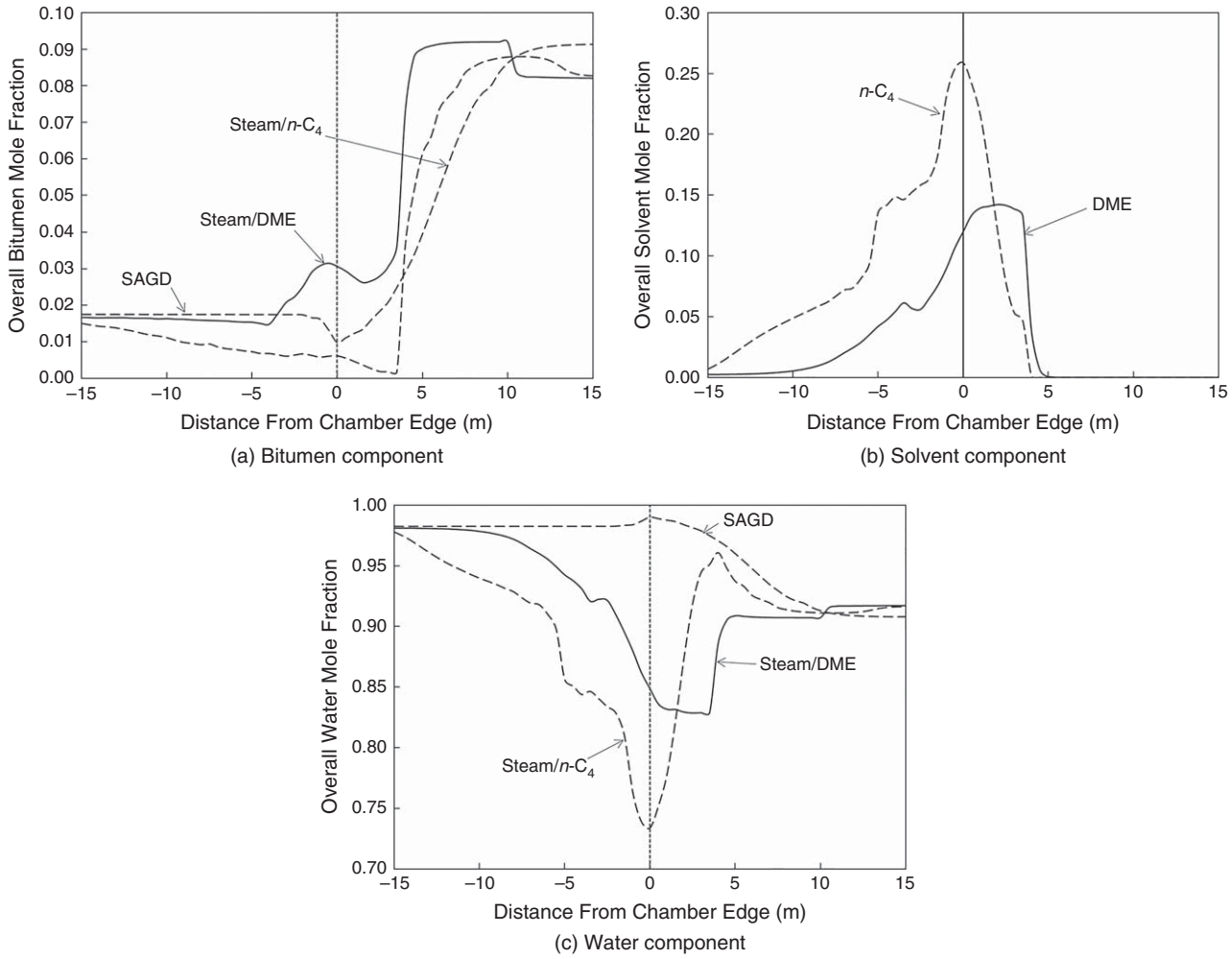

Fig. B-6—Profiles of overall compositions for C_4-SAGD, DME-SAGD, and SAGD at the 24th row from the reservoir top at 1.8 years when four times more gridblocks are used. The vertical line indicates the edge of a steam chamber, the left side of which is the steam chamber. Only the region within 15 m of the chamber edge is shown. (a) Bitumen component; (b) solvent component; (c) water component.

SI Metric Conversion Factors

ft × 3.048*	E−01 = m
bbl × 1.589 873*	E−01 = m^3
bar × 1.0*	E+05 = Pa
psi × 6.894 757*	E+00 = kPa
°F (°F+459.67)/1.8	= K

*Conversion factor is exact.

Kai Sheng is a PhD degree candidate in petroleum engineering in the Hildebrand Department of Petroleum and Geosystems Engineering at the University of Texas at Austin. His research interests include thermal EOR, numerical reservoir simulation, multiphase behavior, and fluid properties of heavy oil and bitumen. Sheng holds a bachelor's degree from the China University of Petroleum (East China) and a master's degree from the University of Alberta, Canada, both in petroleum engineering. He is a member of SPE.

Ryosuke Okuno is an assistant professor in the Hildebrand Department of Petroleum and Geosystems Engineering at the University of Texas at Austin. Before his current position, he served as an assistant professor of petroleum engineering at the University of Alberta from 2010 to 2015. Okuno has 7 years of industrial experience as a reservoir engineer with Japan Petroleum Exploration Company Limited, and is a registered professional engineer in Alberta, Canada. His research and teaching interests include EOR, heavy-oil recovery, unconventional resources, numerical-reservoir simulation, thermodynamics, multiphase behavior, and applied mathematics. Okuno holds bachelor's and master's degrees in geosystem engineering from the University of Tokyo, and a PhD degree in petroleum engineering from the University of Texas at Austin. He is a recipient of the 2012 SPE Petroleum Engineering Junior Faculty Research Initiation Award, is an associate editor for *SPE Journal*, and holds the Pioneer Corporation Faculty Fellowship in Petroleum Engineering at the University of Texas at Austin.

Mingyuan Wang is a PhD degree candidate in petroleum engineering in the Hildebrand Department of Petroleum and Geosystems Engineering at the University of Texas at Austin. His current research interests include EOR, tight oil recovery, and numerical reservoir simulation. Wang holds a bachelor's degree from the China University of Petroleum (Beijing) and a master's degree from the University of Alberta, both in petroleum engineering. He is a member of SPE.